Chapter 2

Wave-Equation Description of Nonlinear Optical Interactions

2.1 The Wave Equation for Nonlinear Optical Media

We have seen in the last chapter how nonlinearity in the response of a material system to an intense laser field can cause the polarization of the medium to develop new frequency components not present in the incident radiation field. These new frequency components of the nonlinear polarization act as sources of new frequency components of the electromagnetic field. In the present chapter, we examine how Maxwell's equations describe the generation of these new components, and more generally we see how the various frequency components of the field become coupled by the nonlinear interaction.

Before developing the mathematical theory of these effects, we give a simple physical picture of how these frequency components are generated. For definiteness, we consider the case of sum-frequency generation as shown in part (a) of Fig. 2.1.1, where the input fields are at frequencies ω_1 and ω_2. Because of nonlinearities in the atomic response, each atom develops an oscillating dipole moment that contains a component at frequency $\omega_1 + \omega_2$. An isolated atom would radiate at this frequency in the form of a dipole radiation pattern, as shown symbolically in part (b) of the figure. However, any material sample contains an enormous number N of atomic dipoles, each oscillating with a phase that is determined by the phases of the incident fields. If the relative phasing of these dipoles is correct, the field radiated by each dipole will add constructively in the forward direction, leading to radiation in the form of a well-defined beam, as illustrated in part (c) of the figure. The system will act as a phased array of dipoles when a certain condition, known as the phase-matching condition (see Eq. (2.2.14) in the next section), is satisfied. Under these conditions, the electric field strength of the radiation emitted in the forward direction will be N times larger than that due to any one atom, and consequently the intensity will be N^2 times as large.

Let us now consider the form of the wave equation for the propagation of light through a nonlinear optical medium. We begin with Maxwell's equations, which we write in SI units in

Nonlinear Optics. https://doi.org/10.1016/B978-0-12-811002-7.00011-4

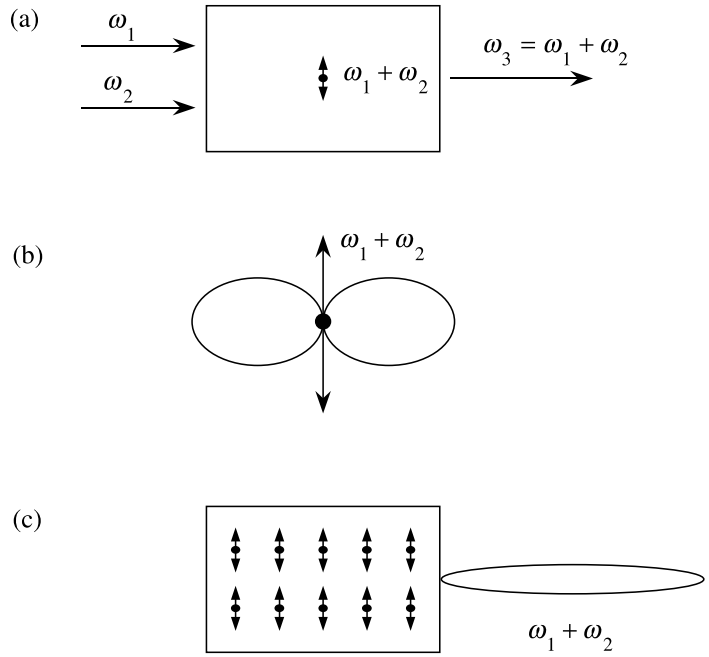

FIGURE 2.1.1: Sum-frequency generation.

the form*

$$\nabla \cdot \tilde{\mathbf{D}} = \tilde{\rho}, \tag{2.1.1}$$

$$\nabla \cdot \tilde{\mathbf{B}} = 0, \tag{2.1.2}$$

$$\nabla \times \tilde{\mathbf{E}} = -\frac{\partial \tilde{\mathbf{B}}}{\partial t}, \tag{2.1.3}$$

$$\nabla \times \tilde{\mathbf{H}} = \frac{\partial \tilde{\mathbf{D}}}{\partial t} + \tilde{\mathbf{J}}. \tag{2.1.4}$$

We are primarily interested in the solution of these equations in regions of space that contain no free charges, so that

$$\tilde{\rho} = 0, \tag{2.1.5}$$

and that contain no free currents, so that

$$\tilde{\mathbf{J}} = 0. \tag{2.1.6}$$

* Throughout the text we use a tilde (~) to denote a quantity that varies rapidly in time.

We also assume that the material is nonmagnetic, so that

$$\tilde{\mathbf{B}} = \mu_0 \tilde{\mathbf{H}}. \tag{2.1.7}$$

However, we allow the material to be nonlinear in the sense that the fields $\tilde{\mathbf{D}}$ and $\tilde{\mathbf{E}}$ are related by

$$\tilde{\mathbf{D}} = \epsilon_0 \tilde{\mathbf{E}} + \tilde{\mathbf{P}}, \tag{2.1.8}$$

where in general the polarization vector $\tilde{\mathbf{P}}$ depends nonlinearly upon the local value of the electric field strength $\tilde{\mathbf{E}}$.

We now proceed to derive the optical wave equation in the usual manner. We take the curl of the curl-$\tilde{\mathbf{E}}$ Maxwell equation (2.1.3), interchange the order of space and time derivatives on the right-hand side of the resulting equation, and use Eqs. (2.1.4), (2.1.6), and (2.1.7) to replace $\nabla \times \tilde{\mathbf{B}}$ by $\mu_0(\partial \tilde{\mathbf{D}}/\partial t)$, to obtain the equation

$$\nabla \times \nabla \times \tilde{\mathbf{E}} + \mu_0 \frac{\partial^2}{\partial t^2} \tilde{\mathbf{D}} = 0. \tag{2.1.9a}$$

We now use Eq. (2.1.8) to eliminate $\tilde{\mathbf{D}}$ from this equation, and we thereby obtain the expression

$$\nabla \times \nabla \times \tilde{\mathbf{E}} + \frac{1}{c^2} \frac{\partial^2}{\partial t^2} \tilde{\mathbf{E}} = -\frac{1}{\epsilon_0 c^2} \frac{\partial^2 \tilde{\mathbf{P}}}{\partial t^2}. \tag{2.1.9b}$$

On the right-hand side of this equation we have replaced μ_0 by $1/\epsilon_0 c^2$ for future convenience.

This is the most general form of the wave equation in nonlinear optics. Under certain conditions it can be simplified. For example, by using an identity from vector calculus, we can write the first term on the left-hand side of Eq. (2.1.9b) as

$$\nabla \times \nabla \times \tilde{\mathbf{E}} = \nabla\big(\nabla \cdot \tilde{\mathbf{E}}\big) - \nabla^2 \tilde{\mathbf{E}}. \tag{2.1.10}$$

In the linear optics of isotropic source-free media, the first term on the right-hand side of this equation vanishes because the Maxwell equation $\nabla \cdot \tilde{\mathbf{D}} = 0$ implies that $\nabla \cdot \tilde{\mathbf{E}} = 0$. However, in nonlinear optics this term is generally nonvanishing even for isotropic materials, as a consequence of the more general relation (2.1.8) between $\tilde{\mathbf{D}}$ and $\tilde{\mathbf{E}}$. Fortunately, in nonlinear optics the first term on the right-hand side of Eq. (2.1.10) can usually be dropped for cases of interest. For example, if $\tilde{\mathbf{E}}$ is of the form of a transverse, infinite plane wave, $\nabla \cdot \tilde{\mathbf{E}}$ vanishes identically. More generally, the first term can often be shown to be small, even when it does not vanish identically, especially when the slowly varying amplitude approximation (see Section 2.2) is valid. For the remainder of this book, we shall usually assume that the contribution of $\nabla(\nabla \cdot \tilde{\mathbf{E}})$ in Eq. (2.1.10) is negligible so that the wave equation can be taken to have the form

$$\nabla^2 \tilde{\mathbf{E}} - \frac{1}{c^2} \frac{\partial^2}{\partial t^2} \tilde{\mathbf{E}} = \frac{1}{\epsilon_0 c^2} \frac{\partial^2 \tilde{\mathbf{P}}}{\partial t^2}. \tag{2.1.11}$$

Alternatively, the wave equation can be expressed as

$$\nabla^2\tilde{\mathbf{E}} - \frac{1}{\epsilon_0 c^2}\frac{\partial^2}{\partial t^2}\tilde{\mathbf{D}} = 0 \tag{2.1.12}$$

where $\tilde{\mathbf{D}} = \epsilon_0\tilde{\mathbf{E}} + \tilde{\mathbf{P}}$.

It is often convenient to split $\tilde{\mathbf{P}}$ into its linear and nonlinear parts as

$$\tilde{\mathbf{P}} = \tilde{\mathbf{P}}^{(1)} + \tilde{\mathbf{P}}^{\mathrm{NL}}. \tag{2.1.13}$$

Here $\tilde{\mathbf{P}}^{(1)}$ is the part of $\tilde{\mathbf{P}}$ that depends linearly on the electric field strength $\tilde{\mathbf{E}}$. We can similarly decompose the displacement field $\tilde{\mathbf{D}}$ into its linear and nonlinear parts as

$$\tilde{\mathbf{D}} = \tilde{\mathbf{D}}^{(1)} + \tilde{\mathbf{P}}^{\mathrm{NL}}, \tag{2.1.14a}$$

where the linear part is given by

$$\tilde{\mathbf{D}}^{(1)} = \epsilon_0\tilde{\mathbf{E}} + \tilde{\mathbf{P}}^{(1)}. \tag{2.1.14b}$$

In terms of this quantity, the wave equation (2.1.11) can be written as

$$\nabla^2\tilde{\mathbf{E}} - \frac{1}{\epsilon_0 c^2}\frac{\partial^2\tilde{\mathbf{D}}^{(1)}}{\partial t^2} = \frac{1}{\epsilon_0 c^2}\frac{\partial^2\tilde{\mathbf{P}}^{\mathrm{NL}}}{\partial t^2}. \tag{2.1.15}$$

To see why this form of the wave equation is useful, let us first consider the case of a lossless, dispersionless medium. We can then express the relation between $\tilde{\mathbf{D}}^{(1)}$ and $\tilde{\mathbf{E}}$ in terms of a real, frequency-independent dielectric tensor $\boldsymbol{\epsilon}^{(1)}$ as

$$\tilde{\mathbf{D}}^{(1)} = \epsilon_0\boldsymbol{\epsilon}^{(1)}\cdot\tilde{\mathbf{E}}. \tag{2.1.16a}$$

For the case of an isotropic material, this relation reduces to simply

$$\tilde{\mathbf{D}}^{(1)} = \epsilon_0\epsilon^{(1)}\tilde{\mathbf{E}}, \tag{2.1.16b}$$

where $\epsilon^{(1)}$ is a scalar quantity. Note that we are using the convention that $\epsilon_0 = 8.85 \times 10^{-12}$ F/m is a fundamental constant, the permittivity of free space, whereas $\epsilon^{(1)}$ is the dimensionless, relative permittivity which is different for each material. For this (simpler) case of an isotropic, dispersionless material, the wave equation (2.1.15) becomes

$$\nabla^2\tilde{\mathbf{E}} - \frac{\epsilon^{(1)}}{c^2}\frac{\partial^2\tilde{\mathbf{E}}}{\partial t^2} = \frac{1}{\epsilon_0 c^2}\frac{\partial^2\tilde{\mathbf{P}}^{\mathrm{NL}}}{\partial t^2}. \tag{2.1.17}$$

This equation has the form of a driven (i.e., inhomogeneous) wave equation; the nonlinear response of the medium acts as a source term that appears on the right-hand side of this equation. In the absence of this source term, Eq. (2.1.17) admits solutions of the form of free

waves propagating with velocity c/n, where n is the (linear) index of refraction that satisfies $n^2 = \epsilon^{(1)}$.

For the case of a dispersive medium, we must consider each frequency component of the field separately. We represent the electric, linear displacement, and polarization fields as the sums of their various frequency components:

$$\tilde{\mathbf{E}}(\mathbf{r}, t) = \sum_n{}' \tilde{\mathbf{E}}_n(\mathbf{r}, t), \tag{2.1.18a}$$

$$\tilde{\mathbf{D}}^{(1)}(\mathbf{r}, t) = \sum_n{}' \tilde{\mathbf{D}}_n^{(1)}(\mathbf{r}, t), \tag{2.1.18b}$$

$$\tilde{\mathbf{P}}^{\mathrm{NL}}(\mathbf{r}, t) = \sum_n{}' \tilde{\mathbf{P}}_n^{\mathrm{NL}}(\mathbf{r}, t), \tag{2.1.18c}$$

where the summation is to be performed over positive field frequencies only, and we represent each frequency component in terms of its complex amplitude as

$$\tilde{\mathbf{E}}_n(\mathbf{r}, t) = \mathbf{E}_n(\mathbf{r}) e^{-i\omega_n t} + \text{c.c.}, \tag{2.1.19a}$$

$$\tilde{\mathbf{D}}_n^{(1)}(\mathbf{r}, t) = \mathbf{D}_n^{(1)}(\mathbf{r}) e^{-i\omega_n t} + \text{c.c.}, \tag{2.1.19b}$$

$$\tilde{\mathbf{P}}_n^{\mathrm{NL}}(\mathbf{r}, t) = \mathbf{P}_n^{\mathrm{NL}}(\mathbf{r}) e^{-i\omega_n t} + \text{c.c.} \tag{2.1.19c}$$

If dissipation can be neglected, the relationship between $\tilde{\mathbf{D}}_n^{(1)}$ and $\tilde{\mathbf{E}}_n$ can be expressed in terms of a real, frequency-dependent dielectric tensor according to

$$\tilde{\mathbf{D}}_n^{(1)}(\mathbf{r}, t) = \epsilon_0 \boldsymbol{\epsilon}^{(1)}(\omega_n) \cdot \tilde{\mathbf{E}}_n(\mathbf{r}, t). \tag{2.1.20}$$

When Eqs. (2.1.18a) through (2.1.20) are introduced into the wave equation in the form of (2.1.15), we obtain a wave equation analogous to (2.1.17) that is valid for each frequency component of the field:

$$\nabla^2 \tilde{\mathbf{E}}_n - \frac{\boldsymbol{\epsilon}^{(1)}(\omega_n)}{c^2} \cdot \frac{\partial^2 \tilde{\mathbf{E}}_n}{\partial t^2} = \frac{1}{\epsilon_0 c^2} \frac{\partial^2 \tilde{\mathbf{P}}_n^{\mathrm{NL}}}{\partial t^2}. \tag{2.1.21}$$

The general case of a dissipative medium is treated by allowing the dielectric tensor to be a complex quantity that relates the complex field amplitudes according to

$$\mathbf{D}_n^{(1)}(\mathbf{r}) = \epsilon_0 \boldsymbol{\epsilon}^{(1)}(\omega_n) \cdot \mathbf{E}_n(\mathbf{r}). \tag{2.1.22}$$

This expression, along with Eqs. (2.1.18) and (2.1.19), can be introduced into the wave equation (2.1.15), to obtain

$$\nabla^2 \mathbf{E}_n(\mathbf{r}) + \frac{\omega_n^2}{c^2} \boldsymbol{\epsilon}^{(1)}(\omega_n) \cdot \mathbf{E}_n(\mathbf{r}) = -\frac{\omega_n^2}{\epsilon_0 c^2} \mathbf{P}_n^{\mathrm{NL}}(\mathbf{r}). \tag{2.1.23}$$

This equation is the frequency-domain version of the wave equation and is often referred to as a Helmholtz equation.

2.2 The Coupled-Wave Equations for Sum-Frequency Generation

We next study how the nonlinear optical wave equation that we derived in the previous section can be used to describe specific nonlinear optical interactions. In particular, we consider sum-frequency generation in a lossless nonlinear optical medium involving collimated, monochromatic, continuous-wave input beams. We assume the configuration shown in Fig. 2.2.1, where the applied waves fall onto the nonlinear medium at normal incidence. For simplicity, we ignore double refraction effects. The treatment given here can be generalized straightforwardly to include nonnormal incidence and double refraction.*

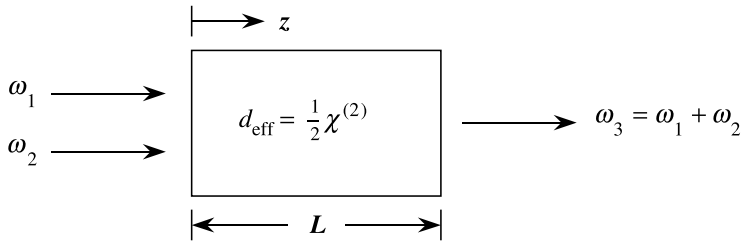

FIGURE 2.2.1: Sum-frequency generation.

The wave equation in Eq. (2.1.21) must hold for each frequency component of the field and in particular for the sum-frequency component at frequency ω_3. In the absence of a nonlinear source term, the solution to this equation for a plane wave at frequency ω_3 propagating in the $+z$ direction is

$$\tilde{E}_3(z,t) = A_3 e^{i(k_3 z - \omega_3 t)} + \text{c.c.}, \tag{2.2.1}$$

where†

$$k_3 = \frac{n_3 \omega_3}{c}, \quad n_3^2 = \epsilon^{(1)}(\omega_3), \tag{2.2.2}$$

and where the amplitude of the wave A_3 is a *constant*. We expect on physical grounds that, when the nonlinear source term is not too large, the solution to Eq. (2.1.21) will still be of the form of Eq. (2.2.1), except that A_3 will become a slowly varying function of z. We hence adopt Eq. (2.2.1) with A_3 taken to be a function of z as the form of the trial solution to the wave equation (2.1.21) in the presence of the nonlinear source term.

We represent the nonlinear source term appearing in Eq. (2.1.21) as

$$\tilde{P}_3(z,t) = P_3 e^{-i\omega_3 t} + \text{c.c.}, \tag{2.2.3}$$

* See, for example, Shen (1984a), Chapter 6.

† For convenience, we are working in the scalar field approximation; n_3 represents the refractive index appropriate to the state of polarization of the ω_3 wave.

where according to Eq. (1.5.28)

$$P_3 = 4\epsilon_0 d_{\text{eff}} E_1 E_2. \tag{2.2.4}$$

We represent the applied fields ($i = 1, 2$) as

$$\tilde{E}_i(z,t) = E_i e^{-i\omega_i t} + \text{c.c.}, \quad \text{where} \quad E_i = A_i e^{ik_i z}. \tag{2.2.5}$$

The amplitude of the nonlinear polarization can then be written as

$$P_3 = 4\epsilon_0 d_{\text{eff}} A_1 A_2 e^{i(k_1+k_2)z} \equiv p_3 e^{i(k_1+k_2)z}. \tag{2.2.6}$$

We now substitute Eqs. (2.2.1), (2.2.3), and (2.2.6) into the wave equation (2.1.21). Since the fields depend only on the longitudinal coordinate z, we can replace ∇^2 by d^2/dz^2. We then obtain

$$\left[\frac{d^2A_3}{dz^2} + 2ik_3\frac{dA_3}{dz} - k_3^2 A_3 + \frac{\epsilon^{(1)}(\omega_3)\omega_3^2 A_3}{c^2}\right] e^{i(k_3 z - \omega_3 t)} + \text{c.c.}$$
$$= \frac{-4d_{\text{eff}}\omega_3^2}{c^2} A_1 A_2 e^{i[(k_1+k_2)z - \omega_3 t]} + \text{c.c.} \tag{2.2.7}$$

Since $k_3^2 = \epsilon^{(1)}(\omega_3)\omega_3^2/c^2$, the third and fourth terms on the left-hand side of this expression cancel. Note that we can drop the complex conjugate terms from each side and still maintain the equality. We can then cancel the factor $\exp(-i\omega_3 t)$ on each side and write the resulting equation as

$$\frac{d^2A_3}{dz^2} + 2ik_3\frac{dA_3}{dz} = \frac{-4d_{\text{eff}}\omega_3^2}{c^2} A_1 A_2 e^{i(k_1+k_2-k_3)z}. \tag{2.2.8}$$

It is usually permissible to neglect the first term on the left-hand side of this equation on the grounds that it is very much smaller than the second. This approximation is known as the slowly varying amplitude approximation and is valid whenever

$$\left|\frac{d^2A_3}{dz^2}\right| \ll \left|k_3\frac{dA_3}{dz}\right|. \tag{2.2.9}$$

This condition requires that the fractional change in A_3 in a distance of the order of an optical wavelength must be much smaller than unity. When this approximation is made, Eq. (2.2.8) becomes

$$\frac{dA_3}{dz} = \frac{2id_{\text{eff}}\omega_3}{n_3 c} A_1 A_2 e^{i\Delta k z}, \tag{2.2.10}$$

where n_3 is the refractive index experienced by the ω_3 wave and where we have introduced the quantity

$$\Delta k = k_1 + k_2 - k_3, \tag{2.2.11}$$

which is called the wavevector (or momentum) mismatch. Equation (2.2.10) is known as a coupled-amplitude equation, because it shows how the amplitude of the ω_3 wave varies as a consequence of its coupling to the ω_1 and ω_2 waves. In general, the spatial variation of the ω_1 and ω_2 waves must also be taken into consideration, and we can derive analogous equations for the ω_1 and ω_2 fields by repeating the derivation given above for each of these frequencies. We hence find two additional coupled-amplitude equations given by

$$\frac{dA_1}{dz} = \frac{2id_{\text{eff}}\omega_1}{n_1 c} A_3 A_2^* e^{-i\Delta kz}, \tag{2.2.12a}$$

$$\frac{dA_2}{dz} = \frac{2id_{\text{eff}}\omega_2}{n_2 c} A_3 A_1^* e^{-i\Delta kz}. \tag{2.2.12b}$$

Note that, in writing these equations in the forms shown, we have assumed that the medium is lossless. For a lossless medium, no explicit loss terms need be included in these equations, and furthermore we can make use of the condition of full permutation symmetry (Eq. (1.5.8)) to conclude that the coupling coefficient d_{eff} has the same value in each equation.

For future reference, we note that Eq. (2.2.10) can be written more generally in terms of the slowly varying amplitude p_3 of the nonlinear polarization as

$$\frac{dA_3}{dz} = \frac{i\omega_3}{2\epsilon_0 n_3 c} p_3 e^{i\Delta kz}, \tag{2.2.13}$$

where according to Eq. (2.2.6) p_3 is given by $P_3 = p_3 \exp[i(k_1 + k_2)z]$. Analogous equations can of course be written for the spatial variations of A_1 and A_2.

2.2.1 Phase-Matching Considerations

For simplicity, let us assume that the amplitudes A_1 and A_2 of the input fields can be taken as constants on the right-hand side of Eq. (2.2.10). This assumption is valid whenever the conversion of the input fields into the sum-frequency field is not too large. We note that, for the special case

$$\Delta k = 0, \tag{2.2.14}$$

the amplitude A_3 of the sum-frequency wave increases linearly with z, and consequently that its intensity increases quadratically with z. The condition (2.2.14) is known as the condition of perfect phase matching. When this condition is fulfilled, the generated wave maintains a fixed phase relation with respect to the nonlinear polarization and is able to extract energy most efficiently from the incident waves. From a microscopic point of view, when the condition (2.2.14) is fulfilled the individual atomic dipoles that constitute the material system are properly phased so that the field emitted by each dipole adds coherently in the forward direction. The

total power radiated by the ensemble of atomic dipoles thus scales as the square of the number of atoms that participate.

When the condition (2.2.14) is not satisfied, the intensity of the emitted radiation is smaller than for the case of $\Delta k = 0$. The amplitude of the sum-frequency (ω_3) field at the exit plane of the nonlinear medium is obtained in this case by integrating Eq. (2.2.10) from $z = 0$ to $z = L$, yielding

$$A_3(L) = \frac{2id_{\text{eff}}\omega_3 A_1 A_2}{n_3 c}\int_0^L e^{i\Delta kz}\,dz = \frac{2id_{\text{eff}}\omega_3 A_1 A_2}{n_3 c}\left(\frac{e^{i\Delta kL}-1}{i\Delta k}\right). \tag{2.2.15}$$

The intensity of the ω_3 wave is given by the magnitude of the time-averaged Poynting vector, which for our definition of field amplitude is given by

$$I_i = 2n_i\epsilon_0 c|A_i|^2, \quad i = 1, 2, 3. \tag{2.2.16}$$

We thus find that the intensity of the generated wave is given by

$$I_3 = \frac{8n_3\epsilon_0 d_{\text{eff}}^2\omega_3^2|A_1|^2|A_2|^2}{n_3^2 c}\left|\frac{e^{i\Delta kL}-1}{\Delta k}\right|^2. \tag{2.2.17}$$

The squared modulus that appears in this equation can be expressed as

$$\begin{aligned}\left|\frac{e^{i\Delta kL}-1}{\Delta k}\right|^2 &= L^2\left(\frac{e^{i\Delta kL}-1}{\Delta kL}\right)\left(\frac{e^{-i\Delta kL}-1}{\Delta kL}\right) = 2L^2\frac{(1-\cos\Delta kL)}{(\Delta kL)^2}\\ &= L^2\frac{\sin^2(\Delta kL/2)}{(\Delta kL/2)^2} \equiv L^2\,\text{sinc}^2(\Delta kL/2).\end{aligned} \tag{2.2.18}$$

Finally, our expression for I_3 can be written in terms of the intensities of the incident fields by using Eq. (2.2.16) to express $|A_i|^2$ in terms of the intensities, yielding the result

$$I_3 = \frac{2d_{\text{eff}}^2\omega_3^2 I_1 I_2}{n_1 n_2 n_3\epsilon_0 c^3}L^2\,\text{sinc}^2\left(\frac{\Delta kL}{2}\right). \tag{2.2.19}$$

Note that the effect of wavevector mismatch is included entirely in the factor $\text{sinc}^2(\Delta kL/2)$. This phase mismatch factor is plotted in Fig. 2.2.2.

It should be noted that the efficiency of the three-wave mixing process decreases as $|\Delta k|L$ increases, with some oscillations occurring. The reason for this behavior is that if L is greater than approximately $1/\Delta k$, the output wave can get out of phase with its driving polarization, and power can flow from the ω_3 wave back into the ω_1 and ω_2 waves (see Eq. (2.2.10)). For this reason, one sometimes defines

$$L_{\text{coh}} = 2/\Delta k \tag{2.2.20}$$

to be the coherent buildup length of the interaction, so that the phase mismatch factor in Eq. (2.2.19) can be written as

$$\text{sinc}^2(L/L_{\text{coh}}). \tag{2.2.21}$$

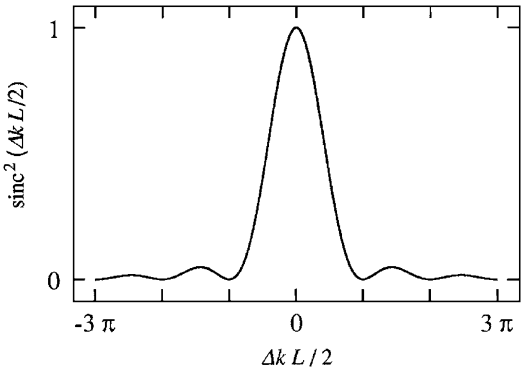

FIGURE 2.2.2: Effects of wavevector mismatch on the efficiency of sum-frequency generation.

2.3 Phase Matching

We saw in Section 2.2 that for sum-frequency generation involving undepleted input beams, the intensity of the generated field at frequency $\omega_3 = \omega_1 + \omega_2$ varies with the wavevector mismatch

$$\Delta k = k_1 + k_2 - k_3 \tag{2.3.1}$$

according to

$$I_3 = I_3^{(\max)} \left[\frac{\sin(\Delta k L/2)}{(\Delta k L/2)} \right]^2. \tag{2.3.2}$$

This expression predicts a drastic decrease in the efficiency of the sum-frequency generation process when the condition of perfect phase matching, $\Delta k = 0$, is not satisfied.

For nonlinear mixing processes that are sufficiently efficient to lead to depletion of the input beams, the functional dependence of the efficiency of the process on the phase mismatch is no longer given by Eq. (2.3.2). However, even in this case the efficient generation of the output field requires that the condition $\Delta k = 0$ be maintained.

Behavior of the sort predicted by Eq. (2.3.2) was first observed experimentally by Maker et al. (1962) and is illustrated in Fig. 2.3.1. Their experiment involved focusing the output of a pulsed ruby laser into a single crystal of quartz and measuring how the intensity of the second-harmonic signal varied as the crystal was rotated, thus varying the effective path length L through the crystal. The wavevector mismatch Δk was nonzero and approximately the same for all orientations used in their experiment.

The phase-matching condition $\Delta k = 0$ is often difficult to achieve because the refractive index of materials that are lossless in the range ω_1 to ω_3 (we assume that $\omega_1 \leq \omega_2 < \omega_3$)

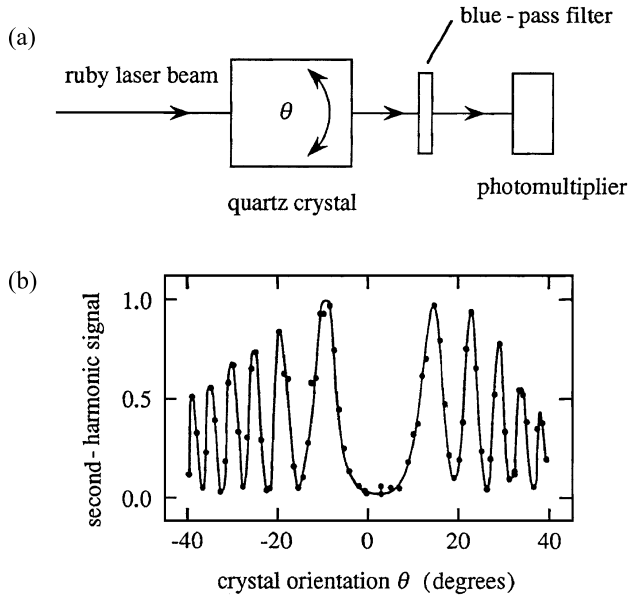

FIGURE 2.3.1: (a) Experimental setup of Maker et al. (b) Their experimental results.

shows an effect known as normal dispersion: the refractive index is an increasing function of frequency. As a result, the condition for perfect phase matching with collinear beams,

$$\frac{n_1\omega_1}{c} + \frac{n_2\omega_2}{c} = \frac{n_3\omega_3}{c}, \tag{2.3.3}$$

where

$$\omega_1 + \omega_2 = \omega_3, \tag{2.3.4}$$

cannot be achieved. For the case of second-harmonic generation, with $\omega_1 = \omega_2$, $\omega_3 = 2\omega_1$, these conditions require that

$$n(\omega_1) = n(2\omega_1), \tag{2.3.5}$$

which is clearly not possible when $n(\omega)$ increases monotonically with ω. For the case of sum-frequency generation, the argument is slightly more complicated, but the conclusion is the same. To show that phase matching is not possible in this case, we first rewrite Eq. (2.3.3) as

$$n_3 = \frac{n_1\omega_1 + n_2\omega_2}{\omega_3}. \tag{2.3.6}$$

This result is now used to express the refractive index difference $n_3 - n_2$ as

$$n_3 - n_2 = \frac{n_1\omega_1 + n_2\omega_2 - n_2\omega_3}{\omega_3} = \frac{n_1\omega_1 - n_2(\omega_3 - \omega_2)}{\omega_3} = \frac{n_1\omega_1 - n_2\omega_1}{\omega_3},$$

or finally as

$$n_3 - n_2 = (n_1 - n_2)\frac{\omega_1}{\omega_3}. \tag{2.3.7}$$

For normal dispersion, n_3 must be greater than n_2, and hence the left-hand side of this equation must be positive. However, n_2 must also be greater than n_1, showing that the right-hand side must be negative, which demonstrates that Eq. (2.3.7) cannot possess a solution.

In principle, it is possible to achieve the phase-matching condition by making use of anomalous dispersion, that is, the decrease in refractive index with increasing frequency that occurs near an absorption feature. However, the most common procedure for achieving phase matching is to make use of use of birefringence, which is displayed by many crystals. Birefringence is the dependence of the refractive index on the direction of polarization of the optical radiation. Not all crystals display birefringence; in particular, crystals belonging to the cubic crystal system are optically isotropic (i.e., show no birefringence) and thus are not phase-matchable by this procedure.

The linear optical properties of the various crystal systems are summarized in Table 2.3.1.

In order to achieve phase matching through the use of birefringent crystals, the highest-frequency wave $\omega_3 = \omega_1 + \omega_2$ is polarized in the direction that gives it the lower of the two possible refractive indices. For the case of a negative uniaxial crystal, as in the example shown in Fig. 2.3.2, this choice corresponds to the extraordinary polarization. There are two choices for the polarizations of the lower-frequency waves. Midwinter and Warner (1965) define type I phase matching to be the case in which the two lower-frequency waves have the same polarization, and type II to be the case where the polarizations are orthogonal. The possibilities are summarized in Table 2.3.2. No assumptions regarding the relative sizes of ω_1 and ω_2 are implied by the classification scheme. However, for type II phase matching it is easier to achieve the phase-matching condition (i.e., less birefringence is required) if $\omega_2 > \omega_1$ for the choice of ω_1 and ω_2 used in writing the table. Also, independent of the relative values of ω_1 and ω_2, type I phase matching is easier to achieve than type II.

TABLE 2.3.1: Linear optical classification of the various crystal systems.

System	Linear Optical Classification
Triclinic, monoclinic, orthorhombic	Biaxial
Trigonal, tetragonal, hexagonal	Uniaxial
Cubic	Isotropic

Careful control of the refractive indices at each of the three optical frequencies is required in order to achieve the phase-matching condition ($\Delta k = 0$). Typically phase matching is accomplished by one of two methods: angle tuning and temperature tuning.

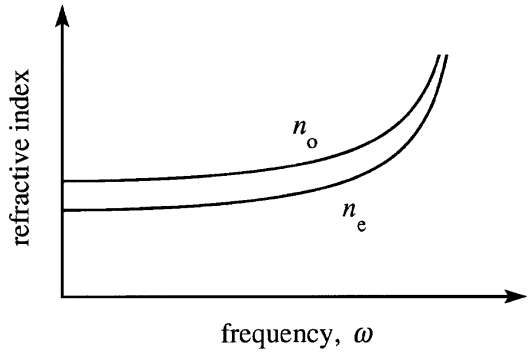

FIGURE 2.3.2: Dispersion of the refractive indices of a negative uniaxial crystal. For the opposite case of a positive uniaxial crystal, the extraordinary index n_e is greater than the ordinary index n_o.

TABLE 2.3.2: Phase-matching methods for uniaxial crystals.

	Positive uniaxial ($n_e > n_0$)	Negative uniaxial ($n_e < n_0$)
Type I	$n_3^o\omega_3 = n_1^e\omega_1 + n_2^e\omega_2$	$n_3^e\omega_3 = n_1^o\omega_1 + n_2^o\omega_2$
Type II	$n_3^o\omega_3 = n_1^o\omega_1 + n_2^e\omega_2$	$n_3^e\omega_3 = n_1^e\omega_1 + n_2^o\omega_2$

Angle Tuning

This method involves precise angular orientation of the crystal with respect to the propagation direction of the incident light. It is most simply described for the case of a uniaxial crystal, and the following discussion is restricted to this case. Uniaxial crystals are characterized by a particular direction known as the optic axis (or c axis or z axis). Light polarized perpendicular to the plane containing the propagation vector $\mathbf{k}$ and the optic axis is called the ordinary polarization. Such light experiences the ordinary refractive index n_o. Light polarized in the plane containing $\mathbf{k}$ and the optic axis is called the extraordinary polarization and experiences a refractive index $n_e(\theta)$ that depends on the angle θ between the optic axis and $\mathbf{k}$ according to the relation*

$$\frac{1}{n_e(\theta)^2} = \frac{\sin^2\theta}{\bar{n}_e^2} + \frac{\cos^2\theta}{n_o^2}. \tag{2.3.8}$$

Here $\bar{n}_e$ is the *principal value* of the extraordinary refractive index. Note that $n_e(\theta)$ is equal to the principal value $\bar{n}_e$ for $\theta = 90$ degrees and is equal to n_o for $\theta = 0$. Phase matching is achieved by adjusting the angle θ to obtain the value of $n_e(\theta)$ for which the condition $\Delta k = 0$ is satisfied.

* For a derivation of this relation, see, for example, Born and Wolf (1975), Section 14.3; Klein (1970), Eq. (11.160a); or Zernike and Midwinter (1973a), Eq. (1.26).

As an illustration of angle phase matching, we consider the case of type I second-harmonic generation in a negative uniaxial crystal, as shown in Fig. 2.3.3. Since n_e is less than n_o for a negative uniaxial crystal, one chooses the fundamental frequency to propagate as an ordinary wave and the second-harmonic frequency to propagate as an extraordinary wave, in order that the birefringence of the material can compensate for the dispersion. The phase-matching condition (2.3.5) then becomes

$$n_e(2\omega, \theta) = n_o(\omega), \tag{2.3.9}$$

or

$$\frac{\sin^2\theta}{\bar{n}_e(2\omega)^2} + \frac{\cos^2\theta}{n_o(2\omega)^2} = \frac{1}{n_o(\omega)^2}. \tag{2.3.10}$$

In order to simplify this equation, we replace $\cos^2\theta$ by $1 - \sin^2\theta$ and solve for $\sin^2\theta$ to obtain

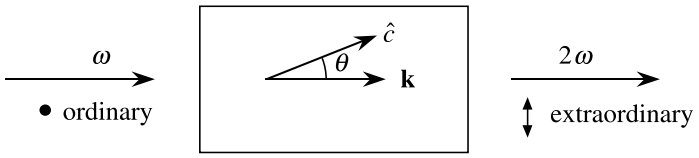

FIGURE 2.3.3: Geometry of angle-tuned phase matching of second-harmonic generation for the case of a negative uniaxial crystal.

$$\sin^2\theta = \frac{\dfrac{1}{n_o(\omega)^2} - \dfrac{1}{n_o(2\omega)^2}}{\dfrac{1}{\bar{n}_e(2\omega)^2} - \dfrac{1}{n_o(2\omega)^2}}. \tag{2.3.11}$$

This equation shows how the crystal should be oriented in order to achieve the phase-matching condition. Note that this equation does not necessarily possess a solution for a physically realizable orientation angle (that is, a real value of the angle θ). For example, if for some material the dispersion in the linear refractive index is too large or the birefringence is too small, the right-hand side of this equation can have a magnitude larger than unity and consequently the equation will have no solution.

The determination of the phase matching angle can be performed as a function of the wavelengths of the two input waves. The results of such a calculation are shown in Fig. 2.3.4 for type-I collinear phase matching in lithium niobate. Lithium niobate is a negative uniaxial crystal, and thus the two longer-wavelength waves have o polarization and the high-frequency wave has e polarization. The label on each curve gives the phase matching angle, that is, the angle between the wavevector of the waves and the optic axis of the crystal. This plot

was obtained through use of the refractive index data of Jundt (1997) and of Edwards and Lawrence (1984) which were analyzed by the commercial software package SNLO (http://www.as-photonics.com/snlo).

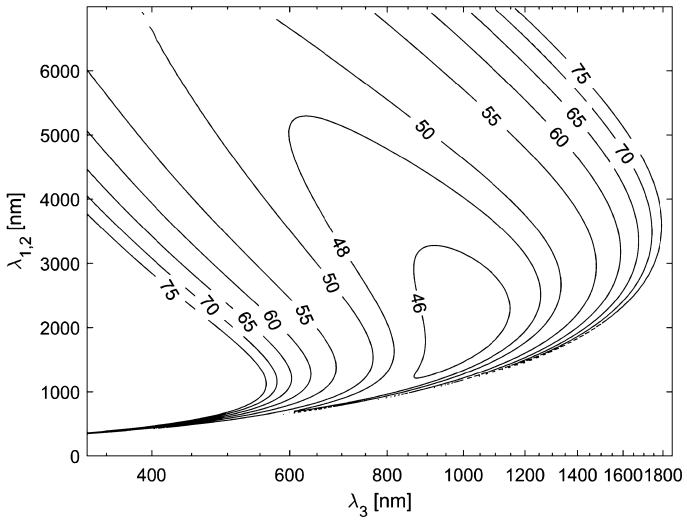

FIGURE 2.3.4: Phase matching curves for type-I collinear phase matching in lithium niobate. Here λ_3 is the wavelength of the wave with the highest frequency, and the low frequency waves have wavelengths λ_1 and λ_2. The number that labels each curve is the phase matching angle in degrees.

Temperature Tuning

There is one serious drawback to the use of angle tuning. Whenever the angle θ between the propagation direction and the optic axis has a value other than 0 or 90 degrees, the Poynting vector **S** and the propagation vector **k** are not parallel for extraordinary rays. As a result, ordinary and extraordinary rays with parallel propagation vectors quickly diverge from one another as they propagate through the crystal. This walkoff effect limits the spatial overlap of the two waves and decreases the efficiency of any nonlinear mixing process involving such waves.

For some crystals, notably lithium niobate, the amount of birefringence is strongly temperature-dependent. As a result, it is possible to phase-match the mixing process by holding θ fixed at 90 degrees and varying the temperature of the crystal. The temperature dependence of the refractive indices of lithium niobate has been given by Hobden and Warner (1966).

2.4 Quasi-Phase-Matching (QPM)

Section 2.3 describes techniques that utilize the birefringence of an optical material to achieve the phase-matching condition of nonlinear optics. This condition must be maintained for the ef-

ficient generation of new frequency components in any nonlinear optical interaction. However, there are circumstances under which these techniques are not suitable. For instance, a particular material may possess no birefringence (an example is gallium arsenide) or may possess insufficient birefringence to compensate for the dispersion of the linear refractive indices over the wavelength range of interest. The problem of insufficient birefringence becomes increasingly acute at shorter wavelengths, because (as illustrated very schematically in Fig. 2.3.2) the refractive index of a given material tends to increase rapidly with frequency at high frequencies, whereas the birefringence (that is, the difference between the ordinary and extraordinary refractive indices) tends to be more nearly constant. Another circumstance under which birefringence phase matching cannot be used is when a particular application requires the use of the d_{33} nonlinear coefficient, which tends to be much larger than the off-diagonal coefficients. For example, for lithium niobate, the d_{31} coefficient is equal to 4.35 pm/V, whereas the d_{33} coefficient is equal to 27 pm/V. However, the d_{33} nonlinear coefficient can be accessed only if all the interacting waves are polarized in the same direction. Under this circumstance, even if birefringence is present it cannot be used to compensate for dispersion.

A technique known as quasi-phase-matching can be used when normal birefringence-based phase matching cannot be implemented. The idea of quasi-phase-matching is illustrated in Fig. 2.4.1, which shows both a single crystal of nonlinear optical material (part (a)) and a periodically poled material (part (b)). A periodically poled material is a structure that has been fabricated in such a manner that the orientation of one of the crystalline axes, often the c axis of a ferroelectric material, is inverted periodically as a function of position within the material. An inversion in the direction of the c axis has the consequence of inverting the sign of the nonlinear coupling coefficient d_{eff}. This periodic alternation of the sign of d_{eff} can compensate for a nonzero wavevector mismatch Δk. The nature of this effect is illustrated in Fig. 2.4.2. Curve (a) of this figure shows that, in a perfectly phase matched interaction in an ordinary single-crystal nonlinear optical material, the field strength of the generated wave grows linearly with propagation distance. In the presence of a wavevector mismatch (curve c), the field amplitude of

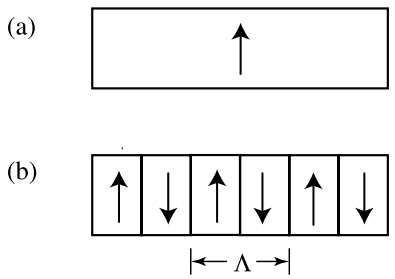

FIGURE 2.4.1: Schematic representations of a second-order nonlinear optical material in the form of (a) a homogeneous single crystal and (b) a periodically poled material in which the positive c axis alternates in orientation with period Λ.

the generated wave oscillates with propagation distance. The nature of quasi-phase-matching is illustrated by curve (b). Here it is assumed that the period Λ of the alternation of the crystalline axis has been set equal to twice the coherent buildup length L_{coh} of the nonlinear interaction. Then, each time the field amplitude of the generated wave is about to begin to decrease as a consequence of the wavevector mismatch, a reversal of the sign of d_{eff} occurs which allows the field amplitude to continue to grow monotonically.

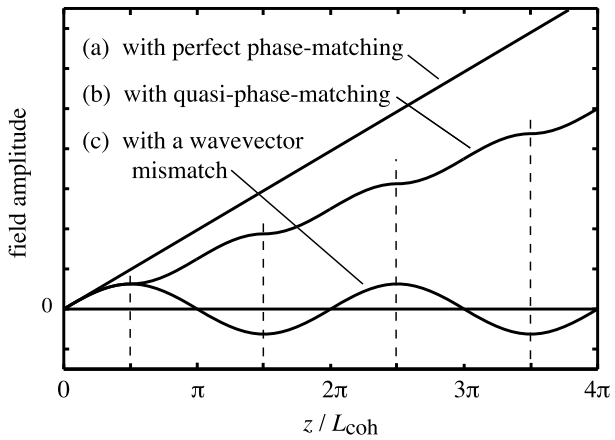

FIGURE 2.4.2: Comparison of the spatial variation of the field amplitude of the generated wave in a nonlinear optical interaction for three different phase matching conditions. Curve (a) assumes that the phase-matching condition is perfectly satisfied, and consequently the field amplitude grows linearly with propagation distance. Curve (c) assumes that the wavevector mismatch Δk is nonzero, and consequently the field amplitude of the generated wave oscillates periodically with distance. Curve (b) assumes the case of a quasi-phase-matched interaction, in which the orientation of the positive c axis is periodically modulated with a period of twice the coherent buildup length L_{coh}, in order to compensate for the influence of wavevector mismatch. In this case the field amplitude grows monotonically with propagation distance, although less rapidly than in the case of a perfectly phase-matched interaction.

A mathematical description of quasi-phase-matching can be formulated as follows. We let $d(z)$ denote the spatial dependence of the nonlinear coupling coefficient. In the example shown in part (b) of Fig. 2.4.1, $d(z)$ is simply the square-wave function which can be represented as

$$d(z) = d_{\text{eff}}\,\text{sign}\big[\cos(2\pi z/\Lambda)\big]; \tag{2.4.1}$$

more complicated spatial variations are also possible. In this equation, d_{eff} denotes the nonlinear coefficient of the homogeneous material. The spatial variation of the nonlinear coefficient leads to a modification of the coupled-amplitude equations describing the nonlinear optical interaction. The nature of the modification can be deduced by noting that, in the derivation of the coupled-amplitude equations, the constant quantity d_{eff} appearing in Eq. (2.2.6) must be

replaced by the spatially varying quantity $d(z)$. It is useful to describe the spatial variation of $d(z)$ in terms of a Fourier series as

$$d(z) = d_{\text{eff}} \sum_{m=-\infty}^{\infty} G_m \exp(i k_m z), \tag{2.4.2}$$

where $k_m = 2\pi m/\Lambda$ is the magnitude of the grating vector associated with the mth Fourier component of $d(z)$. For the form of modulation given in the example of Eq. (2.4.1), the coefficients G_m are readily shown to be given by

$$G_m = (2/m\pi)\sin(m\pi/2), \tag{2.4.3}$$

from which it follows that the fundamental amplitude G_1 is given by $G_1 = 2/\pi$. Coupled-amplitude equations are now derived as in Section 2.2. In performing this derivation, one assumes that one particular Fourier component of $d(z)$ provides the dominant coupling among the interacting waves. After making the slowly varying amplitude approximation, one obtains the set of equations

$$\frac{dA_1}{dz} = \frac{2i\omega_1 d_m}{n_1 c} A_3 A_2^* e^{-i(\Delta k_m - 2k_m)z}, \tag{2.4.4a}$$

$$\frac{dA_2}{dz} = \frac{2i\omega_2 d_m}{n_2 c} A_3 A_1^* e^{-i(\Delta k_m - 2k_m)z}, \tag{2.4.4b}$$

$$\frac{dA_3}{dz} = \frac{2i\omega_3 d_m}{n_3 c} A_1 A_2 e^{i\Delta k_m z}, \tag{2.4.4c}$$

where d_m is the nonlinear coupling coefficient which depends on the Fourier order m according to

$$d_m = d_{\text{eff}} G_m \tag{2.4.5}$$

and where the wavevector mismatch for order m is given by

$$\Delta k_m = k_1 + k_2 - k_3 + k_m. \tag{2.4.6}$$

Note that these coupled-amplitude equations are formally identical to those derived above (that is, Eqs. (2.2.10), (2.2.12a), and (2.2.12b)) for a homogeneous material, but they involve modified values of the nonlinear coupling coefficient d_{eff} and wavevector mismatch Δk. Because of the tendency for d_m to decrease with increasing values of m (see Eq. (2.4.3)), it is most desirable to achieve quasi-phase-matching through use of a first-order ($m = 1$) interaction for which

$$\Delta k_m = k_1 + k_2 - k_3 - 2\pi/\Lambda, \qquad d_m = (2/\pi) d_{\text{eff}}. \tag{2.4.7}$$

From the first of these relations, we see that the optimum period for the quasi-phase-matched structure is given by

$$\Lambda = 2L_{\text{coh}} = 2\pi/(k_1 + k_2 - k_3). \tag{2.4.8}$$

As a numerical example, one finds that L_{coh} is equal to 3.4 μm for second-harmonic generation of radiation at a wavelength of 1.06 μm in lithium niobate.

A number of different approaches have been proposed for the fabrication of quasi-phase-matched structures. The idea of quasi-phase-matching originates in the very early paper by Armstrong et al. (1962), which suggests slicing a nonlinear optical medium into thin segments and rotating alternating segments by 180 degrees. This approach, while feasible (see, for example Szilagyi et al., 1976), is hampered by the required micrometer-scale thinness of the individual layers. A breakthrough came when it was discovered that the procedure for growing lithium niobate crystals from a melt could be controlled so as to obtain a crystal with a periodic modulation of the orientation of the ferroelectric domains and hence in the sign of d_{eff}. QPM was demonstrated in this manner by Feng et al. (1980), Lim et al. (1989), Magel et al. (1990), Fejer et al. (1992), and Myers et al. (1995). A further breakthrough came when Yamada et al. (1993) demonstrated the use of a static electric field to invert the orientation of the ferroelectric domains (and consequently of the crystalline c axis) in a thin sample of lithium niobate. In this approach, a metallic electrode pattern in the form of long stripes is deposited onto the top surface of a lithium niobate crystal, whereas the bottom surface is uniformly coated to act as a ground plane. A static electric field of the order of 21 kV/mm is then applied to the material, which leads to domain reversal only of the material directly under the top electrode. QPM based on periodic poling has also been reported in gallium arsenide (Vodopyanov et al., 2004), potassium titanyl phosphate (KTP) (van der Poel et al., 1990), and lithium tantalate (Meyn and Fejer, 1997). Quasi-phase-matched materials offer promise for many applications of nonlinear optics, some of which are outlined in the review of Byer (1997).

The examples described above involve induced phase matching in materials that possess a second-order $\chi^{(2)}$ nonlinear response. This approach is somewhat related to work aimed at inducing a second-order response in amorphous materials through the application of an intense static electric field. Under certain circumstances, the induced response persists even after the static field is removed. Such effects have been observed in silica glass waveguides (Myers et al., 1991) and in amorphous silicon nitride (Grassani et al., 2019). Furthermore, Khanarian et al. (1990) have demonstrated that polymeric materials can similarly be periodically poled by the application of a static electric field.

2.5 The Manley–Rowe Relations

Let us now consider, from a general point of view, the mutual interaction of three optical waves propagating through a lossless nonlinear optical medium, as illustrated in Fig. 2.5.1.

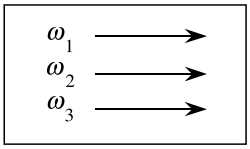

FIGURE 2.5.1: Optical waves of frequencies ω_1, ω_2, and $\omega_3 = \omega_1 + \omega_2$ interact in a lossless nonlinear optical medium.

We have just derived the coupled-amplitude equations (Eqs. (2.2.10) through (2.2.12b)) that describe the spatial variation of the amplitude of each wave. Let us now consider the spatial variation of the *intensity* associated with each of these waves. Since

$$I_i = 2n_i\epsilon_0 c A_i A_i^*, \tag{2.5.1}$$

the variation of the intensity is described by

$$\frac{dI_i}{dz} = 2n_i\epsilon_0 c\left(A_i^*\frac{dA_i}{dz} + A_i\frac{dA_i^*}{dz}\right). \tag{2.5.2}$$

Through use of this result and Eq. (2.2.12a), we find that the spatial variation of the intensity of the wave at frequency ω_1 is given by

$$\begin{aligned}\frac{dI_1}{dz} &= 2n_1\epsilon_0 c\frac{2d_{\text{eff}}\omega_1^2}{k_1c^2}\left(iA_1^*A_3A_2^*e^{-i\Delta kz} + \text{c.c.}\right)\\ &= 4\epsilon_0 d_{\text{eff}}\omega_1\left(iA_3A_1^*A_2^*e^{-i\Delta kz} + \text{c.c.}\right)\end{aligned}$$

or by

$$\frac{dI_1}{dz} = -8\epsilon_0 d_{\text{eff}}\omega_1\,\text{Im}\left(A_3A_1^*A_2^*e^{-i\Delta kz}\right). \tag{2.5.3a}$$

We similarly find that the spatial variation of the intensities of the waves at frequencies ω_2 and ω_3 is given by

$$\frac{dI_2}{dz} = -8\epsilon_0 d_{\text{eff}}\omega_2\,\text{Im}\left(A_3A_1^*A_2^*e^{-i\Delta kz}\right), \tag{2.5.3b}$$

$$\begin{aligned}\frac{dI_3}{dz} &= -8\epsilon_0 d_{\text{eff}}\omega_3\,\text{Im}\left(A_3^*A_1A_2e^{i\Delta kz}\right)\\ &= 8\epsilon_0 d_{\text{eff}}\omega_3\,\text{Im}\left(A_3A_1^*A_2^*e^{-i\Delta kz}\right).\end{aligned} \tag{2.5.3c}$$

We see that the sign of dI_1/dz is the same as that of dI_2/dz but is opposite to that of dI_3/dz. We also see that the direction of energy flow depends on the relative phases of the three interacting fields.

The set of Eqs. (2.5.3) shows that the total power flow is conserved, as expected for propagation through a lossless medium. To demonstrate this fact, we define the total intensity as

$$I = I_1 + I_2 + I_3. \tag{2.5.4}$$

We then find that the spatial variation of the total intensity is given by

$$\begin{aligned}\frac{dI}{dz} &= \frac{dI_1}{dz} + \frac{dI_2}{dz} + \frac{dI_3}{dz} \\ &= -8\epsilon_0 d_{\text{eff}}(\omega_1 + \omega_2 - \omega_3)\,\text{Im}\left(A_3 A_1^* A_2^* e^{-i\Delta kz}\right) = 0,\end{aligned} \tag{2.5.5}$$

where we have made use of Eqs. (2.5.3) and where the last equality follows from the fact that $\omega_3 = \omega_1 + \omega_2$.

The set of Eqs. (2.5.3) also implies that

$$\frac{d}{dz}\left(\frac{I_1}{\omega_1}\right) = \frac{d}{dz}\left(\frac{I_2}{\omega_2}\right) = -\frac{d}{dz}\left(\frac{I_3}{\omega_3}\right), \tag{2.5.6}$$

as can be verified by inspection. These equalities are known as the Manley–Rowe relations (Manley and Rowe, 1959). Since the energy of a photon of frequency ω_i is $\hbar\omega_i$, the quantity I_i/ω_i that appears in these relations is proportional to the intensity of the wave measured in photons per unit area per unit time. The Manley–Rowe relations can alternatively be expressed as

$$\frac{d}{dz}\left(\frac{I_2}{\omega_2} + \frac{I_3}{\omega_3}\right) = 0, \qquad \frac{d}{dz}\left(\frac{I_1}{\omega_1} + \frac{I_3}{\omega_3}\right) = 0, \qquad \frac{d}{dz}\left(\frac{I_1}{\omega_1} - \frac{I_2}{\omega_2}\right) = 0. \tag{2.5.7}$$

These equations can be formally integrated to obtain the three conserved quantities (conserved in the sense that they are spatially invariant) M_1, M_2, and M_3, which are given by

$$M_1 = \frac{I_2}{\omega_2} + \frac{I_3}{\omega_3}, \qquad M_2 = \frac{I_1}{\omega_1} + \frac{I_3}{\omega_3}, \qquad M_3 = \frac{I_1}{\omega_1} - \frac{I_2}{\omega_2}. \tag{2.5.8}$$

These relations tell us that the rate at which photons at frequency ω_1 are created is equal to the rate at which photons at frequency ω_2 are created and is equal to the rate at which photons at frequency ω_3 are destroyed. This result can be understood intuitively by means of the energy level description of a three-wave mixing process, which is shown in Fig. 2.5.2. This diagram shows that, for a lossless medium, the creation of an ω_1 photon must be accompanied by the creation of an ω_2 photon and the annihilation of an ω_3 photon. It seems at first sight surprising that the Manley–Rowe relations should be consistent with this quantum-mechanical interpretation, when our derivation of these relations appears to be entirely classical. Note, however, that our derivation implicitly assumes that the nonlinear susceptibility possesses full permutation symmetry in that we have taken the coupling constant d_{eff} to have the same value in each of the coupled-amplitude equations (2.2.10), (2.2.12a), and (2.2.12b). We remarked

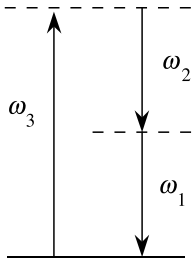

FIGURE 2.5.2: Photon description of the interaction of three optical waves.

earlier (following Eq. (1.5.9)) that in a sense the condition of full permutation symmetry is a consequence of the laws of quantum mechanics.

2.6 Sum-Frequency Generation

In Section 2.2, we treated the process of sum-frequency generation in the simple limit in which the two input fields are undepleted by the nonlinear interaction. In the present section, we treat this process more generally. We assume the configuration shown in Fig. 2.6.1.

The coupled-amplitude equations describing this interaction were derived above and appear as Eqs. (2.2.10) through (2.2.12b). These equations can be solved exactly in terms of the Jacobi elliptic functions. We shall not present the details of this solution, because the method is very similar to the one that we use in Section 2.7 to treat second-harmonic generation. Details can be found in Armstrong et al. (1962); see also Problem 2 at the end of this chapter.

Instead, we treat the somewhat simpler (but more illustrative) case in which one of the applied fields (taken to be at frequency ω_2) is strong, but the other field (at frequency ω_1) is weak. This situation would apply to the conversion of a weak infrared signal of frequency ω_1 to a visible frequency ω_3 by mixing with an intense laser beam of frequency ω_2 (see, for example, Boyd and Townes, 1977a). This process is known as upconversion, because in this process the information-bearing beam is converted to a higher frequency. Usually optical-frequency waves are easier to detect with good sensitivity than are infrared waves. Since we can assume that the

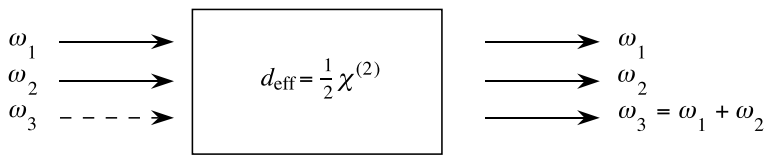

FIGURE 2.6.1: Sum-frequency generation. Typically, no input field is applied at frequency ω_3.

amplitude A_2 of the field at frequency ω_2 is unaffected by the interaction, we can take A_2 to be a constant in the coupled-amplitude equations (Eqs. (2.2.10) through (2.2.12b)), which then reduce to the simpler set

$$\frac{dA_1}{dz} = K_1 A_3 e^{-i\Delta kz}, \tag{2.6.1a}$$

$$\frac{dA_3}{dz} = K_3 A_1 e^{+i\Delta kz}, \tag{2.6.1b}$$

where we have introduced the quantities

$$K_1 = \frac{2i\omega_1^2 d_{\text{eff}}}{k_1 c^2} A_2^*, \qquad K_3 = \frac{2i\omega_3^2 d_{\text{eff}}}{k_3 c^2} A_2, \tag{2.6.2a}$$

and

$$\Delta k = k_1 + k_2 - k_3. \tag{2.6.2b}$$

The solution to Eqs. (2.6.1) is particularly simple if we set $\Delta k = 0$, and we treat this case first. We take the derivative of Eq. (2.6.1a) to obtain

$$\frac{d^2 A_1}{dz^2} = K_1 \frac{dA_3}{dz}. \tag{2.6.3}$$

We now use Eq. (2.6.1b) to eliminate dA_3/dz from the right-hand side of this equation to obtain an equation involving only $A_1(z)$:

$$\frac{d^2 A_1}{dz^2} = -\kappa^2 A_1, \tag{2.6.4}$$

where we have introduced the *positive* coupling coefficient κ^2 defined by

$$\kappa^2 \equiv -K_1 K_3 = \frac{4\omega_1^2 \omega_3^2 d_{\text{eff}}^2 |A_2|^2}{k_1 k_3 c^4}. \tag{2.6.5}$$

The general solution to Eq. (2.6.4) is

$$A_1(z) = B\cos\kappa z + C\sin\kappa z. \tag{2.6.6a}$$

We now obtain the form of $A_3(z)$ through use of Eq. (2.6.1a), which shows that $A_3(z) = (dA_1/dz)/K_1$, or

$$A_3(z) = \frac{-B\kappa}{K_1}\sin\kappa z + \frac{C\kappa}{K_1}\cos\kappa z. \tag{2.6.6b}$$

We next find the solution that satisfies the appropriate boundary conditions. We assume that the ω_3 field is not present at the input, so that the boundary conditions become $A_3(0) = 0$ with

$A_1(0)$ specified. We find from Eq. (2.6.6b) that the boundary condition $A_3(0) = 0$ implies that $C = 0$, and from Eq. (2.6.6a) that $B = A_1(0)$. The solution for the ω_1 field is thus given by

$$A_1(z) = A_1(0)\cos\kappa z \tag{2.6.7}$$

and for the ω_3 field by

$$A_3(z) = -A_1(0)\frac{\kappa}{K_1}\sin\kappa z. \tag{2.6.8}$$

We next express the ratio κ/K_1 as follows:

$$\frac{\kappa}{K_1} = \frac{2\omega_1\omega_3 d_{\text{eff}}|A_2|}{(k_1k_3)^{1/2}c^2}\frac{k_1c^2}{2i\omega_1^2 d_{\text{eff}}A_2^*} = -i\left(\frac{n_1\omega_3}{n_3\omega_1}\right)^{1/2}\frac{|A_2|}{A_2^*}.$$

The ratio $|A_2|/A_2^*$ can be represented as

$$\frac{|A_2|}{A_2^*} = \frac{A_2}{A_2}\frac{|A_2|}{A_2^*} = \frac{A_2|A_2|}{|A_2|^2} = \frac{A_2}{|A_2|} = e^{i\phi_2},$$

where ϕ_2 denotes the phase of A_2. We hence find that

$$A_3(z) = i\left(\frac{n_1\omega_3}{n_3\omega_1}\right)^{1/2}A_1(0)\sin\kappa z e^{i\phi_2}. \tag{2.6.9}$$

The nature of the solution given by Eqs. (2.6.7) and (2.6.9) is illustrated in Fig. 2.6.2.

Let us next solve Eqs. (2.6.1) for the general case of arbitrary wave vector mismatch. We seek a solution to these equations of the form

$$A_1(z) = (Fe^{igz} + Ge^{-igz})e^{-i\Delta kz/2}, \tag{2.6.10}$$

$$A_3(z) = (Ce^{igz} + De^{-igz})e^{i\Delta kz/2}, \tag{2.6.11}$$

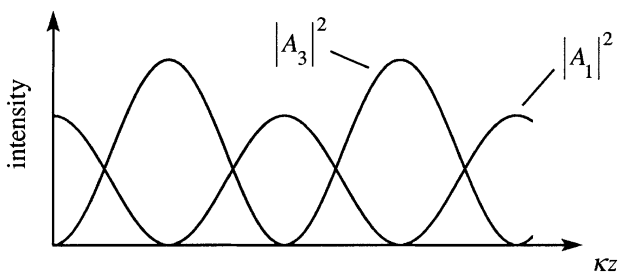

FIGURE 2.6.2: Variation of $|A_1|^2$ and $|A_3|^2$ for the case of perfect phase matching in the undepleted-pump approximation.

where g gives the rate of spatial variation of the fields and where C, D, F, and G are constants whose values depend on the boundary conditions. We take this form for the trial solution because we expect the ω_1 and ω_3 waves to display the same spatial variation, since they are coupled to each other. We separate out the factors $e^{\pm i\Delta kz/2}$ because doing so simplifies the final form of the solution. Equations (2.6.10) and (2.6.11) are now substituted into Eq. (2.6.1a), to obtain

$$\begin{aligned}&\left(igFe^{igz} - igGe^{-igz}\right)e^{-(1/2)i\Delta kz} - \tfrac{1}{2}i\Delta k\left(Fe^{igz} + Ge^{-igz}\right)e^{-(1/2)i\Delta kz}\\ &\quad = \left(K_1Ce^{igz} + K_1De^{-igz}\right)e^{-(1/2)i\Delta kz}.\end{aligned} \tag{2.6.12}$$

Since this equation must hold for all values of z, the terms that vary as e^{igz} and e^{-igz} must each maintain the equality separately; the coefficients of these terms thus must be related by

$$F\left(ig - \tfrac{1}{2}i\Delta k\right) = K_1C, \tag{2.6.13}$$

$$-G\left(ig + \tfrac{1}{2}i\Delta k\right) = K_1D. \tag{2.6.14}$$

In a similar fashion, we find by substituting the trial solution into Eq. (2.6.1b) that

$$\begin{aligned}&\left(igCe^{igz} - igDe^{-igz}\right)e^{(1/2)i\Delta kz} + \tfrac{1}{2}i\Delta k\left(Ce^{igz} + De^{-igz}\right)e^{(1/2)i\Delta kz}\\ &\quad = \left(K_3Fe^{igz} + K_3Ge^{-igz}\right)e^{(1/2)i\Delta kz},\end{aligned} \tag{2.6.15}$$

and in order for this equation to hold for all values of z, the coefficients must satisfy

$$C\left(ig + \tfrac{1}{2}i\Delta k\right) = K_3F, \tag{2.6.16}$$

$$-D\left(ig - \tfrac{1}{2}i\Delta k\right) = K_3G. \tag{2.6.17}$$

Equations (2.6.13) and (2.6.16) constitute simultaneous equations for F and C. We write these equations in matrix form as

$$\begin{bmatrix} i\left(g - \frac{1}{2}\Delta k\right) & -K_1 \\ -K_3 & i\left(g + \frac{1}{2}\Delta k\right) \end{bmatrix} \begin{bmatrix} F \\ C \end{bmatrix} = 0.$$

A solution to this set of equations exists only if the determinant of the matrix of coefficients vanishes, i.e., if

$$g^2 = -K_1K_3 + \tfrac{1}{4}\Delta k^2. \tag{2.6.18}$$

As before (cf. Eq. (2.6.5)), we introduce the positive quantity $\kappa^2 = -K_1K_3$, so that we can express the solution to Eq. (2.6.18) as

$$g = \sqrt{\kappa^2 + \tfrac{1}{4}\Delta k^2}. \tag{2.6.19}$$

In determining g we take only the positive square root in the foregoing expression, since our trial solution (2.6.10) and (2.6.11) explicitly contains both the e^{+gz} and e^{-gz} spatial variations.

The general solution to our original set of equations (2.6.1) is given by Eqs. (2.6.10) and (2.6.11) with g given by Eq. (2.6.19). We evaluate the arbitrary constants C, D, F, and G appearing in the general solution by applying appropriate boundary conditions. We assume that the fields A_1 and A_3 are specified at the input plane $z = 0$ of the nonlinear medium, so that $A_1(0)$ and $A_3(0)$ are known. Then, by evaluating Eqs. (2.6.10) and (2.6.11) at $z = 0$, we find that

$$A_1(0) = F + G, \tag{2.6.20}$$

$$A_3(0) = C + D. \tag{2.6.21}$$

Equations (2.6.13) and (2.6.14) give two additional relations among the quantities C, D, F, and G. Consequently there are four independent linear equations relating the four quantities C, D, F, and G, and their simultaneous solution specifies these four quantities. The values of C, D, F, and G thereby obtained are introduced into the trial solutions (2.6.10) and (2.6.11) to obtain the solution that meets the boundary conditions. This solution is given by

$$A_1(z) = \left[A_1(0)\cos gz + \left(\frac{K_1}{g}A_3(0) + \frac{i\,\Delta k}{2g}A_1(0)\right)\sin gz\right]e^{-(1/2)i\,\Delta kz}, \tag{2.6.22}$$

$$A_3(z) = \left[A_3(0)\cos gz + \left(\frac{-i\,\Delta k}{2g}A_3(0) + \frac{K_3}{g}A_1(0)\right)\sin gz\right]e^{(1/2)i\,\Delta kz}. \tag{2.6.23}$$

In order to interpret this result, let us consider the special case in which no sum-frequency field is incident on the medium, so that $A_3(0) = 0$. Equation (2.6.23) then reduces to

$$A_3(z) = \frac{K_3}{g}A_1(0)\sin gz\, e^{(1/2)i\,\Delta kz} \tag{2.6.24}$$

and the intensity of the generated wave is proportional to

$$\left|A_3(z)\right|^2 = \left|A_1(0)\right|^2\frac{|K_3|^2}{g^2}\sin^2 gz, \tag{2.6.25}$$

where g is given as before by Eq. (2.6.19). We note that the characteristic scale length g^{-1} of the interaction becomes shorter as Δk increases. However, as Δk increases the maximum intensity of the generated wave decreases. Since, according to Eq. (2.6.25), the intensity of the generated wave is inversely proportional to g^2, we see that as Δk is increased the maximum intensity of the generated wave is decreased by the factor $|K_3|^2/(\kappa^2 + \frac{1}{4}\Delta k^2)$. This sort of behavior is illustrated in Fig. 2.6.3, in which the predictions of Eq. (2.6.25) are displayed graphically.

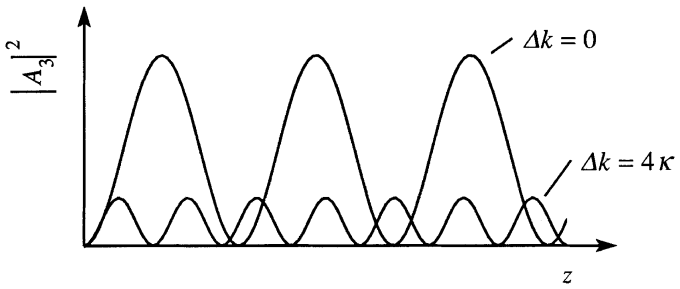

FIGURE 2.6.3: Spatial variation of the sum-frequency wave in the undepleted-pump approximation.

2.7 Second-Harmonic Generation

In this section we present a mathematical description of the process of second-harmonic generation, shown symbolically in Fig. 2.7.1. We assume that the medium is lossless both at the fundamental frequency ω_1 and at the second-harmonic frequency $\omega_2 = 2\omega_1$, so that the nonlinear susceptibility obeys the condition of full permutation symmetry. We treat the interacting waves as plane waves of infinite transverse extent. Our discussion closely follows that of one of the first theoretical treatments of second-harmonic generation (Armstrong et al., 1962).

We take the total electric field within the nonlinear medium to be given by

$$\tilde{E}(z,t) = \tilde{E}_1(z,t) + \tilde{E}_2(z,t), \tag{2.7.1}$$

where each component is expressed in terms of a complex amplitude $E_j(z)$ and slowly varying complex amplitude $A_j(z)$ according to

$$\tilde{E}_j(z,t) = E_j(z)e^{-i\omega_j t} + \text{c.c.}, \tag{2.7.2}$$

for $j = 1, 2$, where

$$E_j(z) = A_j(z)e^{ik_j z}, \tag{2.7.3}$$

and where the propagation constants and refractive indices are given by

$$k_j = n_j\omega_j/c, \quad n_j = \left[\epsilon^{(1)}(\omega_j)\right]^{1/2}. \tag{2.7.4}$$

We assume that each frequency component of the electric field obeys the driven wave equation (see also Eq. (2.1.21))

$$\frac{\partial^2 \tilde{E}_j}{\partial z^2} - \frac{\epsilon^{(1)}(\omega_j)}{c^2}\frac{\partial^2 \tilde{E}_j}{\partial t^2} = \frac{1}{\epsilon_0 c^2}\frac{\partial^2}{\partial t^2}\tilde{P}_j. \tag{2.7.5}$$

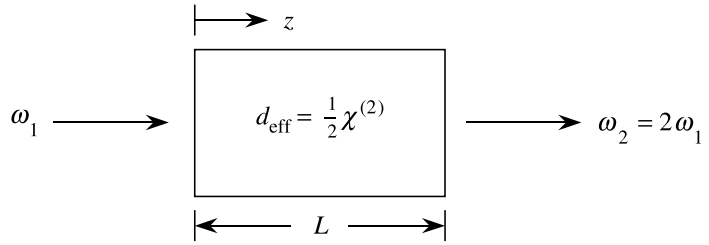

FIGURE 2.7.1: Second-harmonic generation.

The nonlinear polarization is represented as

$$\tilde{P}^{\text{NL}}(z,t) = \tilde{P}_1(z,t) + \tilde{P}_2(z,t) \tag{2.7.6}$$

with

$$\tilde{P}_j(z,t) = P_j(z)e^{-i\omega_j t} + \text{c.c.}, \quad j = 1, 2. \tag{2.7.7}$$

The expressions for the polarization amplitudes are given according to Eqs. (1.5.28) and (1.5.29) by

$$P_1(z) = 4\epsilon_0 d_{\text{eff}} E_2 E_1^* = 4\epsilon_0 d_{\text{eff}} A_2 A_1^* e^{i(k_2 - k_1)z} \tag{2.7.8}$$

and

$$P_2(z) = 2\epsilon_0 d_{\text{eff}} E_1^2 = 2\epsilon_0 d_{\text{eff}} A_1^2 e^{2ik_1 z}. \tag{2.7.9}$$

Note that the degeneracy factors appearing in these two expressions are different. We obtain coupled-amplitude equations for the two frequency components by methods analogous to those used in Section 2.2 in deriving the coupled-amplitude equations for sum-frequency generation. We find that

$$\frac{dA_1}{dz} = \frac{2i\omega_1^2 d_{\text{eff}}}{k_1 c^2} A_2 A_1^* e^{-i\Delta k z} \tag{2.7.10}$$

and

$$\frac{dA_2}{dz} = \frac{i\omega_2^2 d_{\text{eff}}}{k_2 c^2} A_1^2 e^{i\Delta k z}, \tag{2.7.11}$$

where

$$\Delta k = 2k_1 - k_2. \tag{2.7.12}$$

In the undepleted-pump approximation (i.e., A_1 constant), Eq. (2.7.11) can be integrated immediately to obtain an expression for the spatial dependence of the second-harmonic field

amplitude. More generally, the pair of coupled equations must be solved simultaneously. To do so, it is convenient to work with the modulus and phase of each of the field amplitudes rather than with the complex quantities themselves. It is also convenient to express these amplitudes in dimensionless form. To do so, we write the complex, slowly varying field amplitudes as

$$A_1 = \left(\frac{I}{2n_1\epsilon_0 c}\right)^{1/2} u_1 e^{i\phi_1}, \tag{2.7.13}$$

$$A_2 = \left(\frac{I}{2n_2\epsilon_0 c}\right)^{1/2} u_2 e^{i\phi_2}. \tag{2.7.14}$$

Here we have introduced the total intensity of the two waves,

$$I = I_1 + I_2, \tag{2.7.15}$$

where the intensity of each wave is given by

$$I_j = 2n_j\epsilon_0 c|A_j|^2. \tag{2.7.16}$$

As a consequence of the Manley–Rowe relations, the total intensity I is invariant under propagation. The real, normalized field amplitudes u_1 and u_2 are defined such that $u_1^2 + u_2^2$ is also a conserved (i.e., spatially invariant) quantity that satisfies the relation

$$u_1(z)^2 + u_2(z)^2 = 1. \tag{2.7.17}$$

We next introduce a normalized distance parameter

$$\zeta = z/l, \tag{2.7.18}$$

where

$$l = \left(\frac{n_1^2 n_2 \epsilon_0 c}{2I}\right)^{1/2} \frac{c}{\omega_1 d_{\text{eff}}} \tag{2.7.19}$$

is the characteristic distance over which the fields exchange energy. We also introduce the relative phase of the interacting fields,

$$\theta = 2\phi_1 - \phi_2 + \Delta k z, \tag{2.7.20}$$

and a normalized phase-mismatch parameter

$$\Delta s = \Delta k l. \tag{2.7.21}$$

The quantities u_j, ϕ_j, ζ, and Δs defined in Eqs. (2.7.13) through (2.7.21) are now introduced into the coupled-amplitude equations (2.7.10) and (2.7.11), which reduce after straightforward (but lengthy) algebra to the set of coupled equations for the three real quantities u_1, u_2, and θ:

$$\frac{du_1}{d\zeta} = u_1 u_2 \sin\theta, \tag{2.7.22}$$

$$\frac{du_2}{d\zeta} = -u_1^2 \sin\theta, \tag{2.7.23}$$

$$\frac{d\theta}{d\zeta} = \Delta s + \frac{\cos\theta}{\sin\theta}\frac{d}{d\zeta}\left(\ln u_1^2 u_2\right). \tag{2.7.24}$$

This set of equations has been solved under general conditions by Armstrong et al. We shall return later to a discussion of the general solution, but for now we assume the case of perfect phase matching so that Δk and hence Δs vanish. It is easy to verify by direct differentiation that, for $\Delta s = 0$, Eq. (2.7.24) can be rewritten as

$$\frac{d}{d\zeta}\ln\left(u_1^2 u_2 \cos\theta\right) = 0. \tag{2.7.25}$$

Hence the quantity $\ln(\cos\theta u_1^2 u_2)$ is a constant, which we call $\ln\Gamma$, so that the solution to Eq. (2.7.25) can be expressed as

$$u_1^2 u_2 \cos\theta = \Gamma. \tag{2.7.26}$$

The quantity Γ is independent of the normalized propagation distance ζ, and thus the value of Γ can be determined from the known values of u_1, u_2, and θ at the entrance face to the nonlinear medium, $\zeta = 0$.

We have thus found two conserved quantities: $u_1^2 + u_2^2$ (according to Eq. (2.7.17)) and $u_1^2 u_2 \cos\theta$ (according to Eq. (2.7.26)). These conserved quantities can be used to decouple the set of equations (2.7.22)–(2.7.24). Equation (2.7.23), for instance, can be written using Eq. (2.7.17) and the identity $\sin^2\theta + \cos^2\theta = 1$ as

$$\frac{du_2}{d\zeta} = \pm\left(1 - u_2^2\right)\left(1 - \cos^2\theta\right)^{1/2}. \tag{2.7.27}$$

Equations (2.7.26) and (2.7.17) are next used to express $\cos^2\theta$ in terms of the conserved quantity Γ and the unknown function u_2; the resulting expression is substituted into Eq. (2.7.27), which becomes

$$\frac{du_2}{d\zeta} = \pm\left(1 - u_2^2\right)\left(1 - \frac{\Gamma^2}{u_1^4 u_2^2}\right)^{1/2} = \pm\left(1 - u_2^2\right)\left(1 - \frac{\Gamma^2}{(1-u_2^2)^2 u_2^2}\right)^{1/2}. \tag{2.7.28}$$

This result is simplified algebraically to give

$$u_2 \frac{du_2}{d\zeta} = \pm\left[\left(1-u_2^2\right)^2 u_2^2 - \Gamma^2\right]^{1/2},$$

or

$$\frac{du_2^2}{d\zeta} = \pm 2\left[\left(1-u_2^2\right)^2 u_2^2 - \Gamma^2\right]^{1/2}. \tag{2.7.29}$$

This equation is of a standard form, whose solution can be expressed in terms of the Jacobi elliptic functions. An example of the solution for one particular choice of initial conditions is illustrated in Fig. 2.7.2. Note that, in general, the fundamental and second-harmonic fields interchange energy periodically.

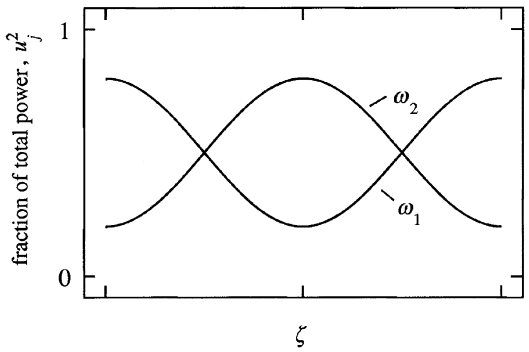

FIGURE 2.7.2: Typical solution to Eq. (2.7.29), after Armstrong et al. (1962).

The solution of Eq. (2.7.29) becomes particularly simple for the special case in which the constant Γ vanishes. The condition $\Gamma = 0$ occurs whenever the amplitude of either of the two input fields is equal to zero or whenever the fields are initially phased so that $\cos\theta = 0$. We note that since Γ is a conserved quantity, it is then equal to zero for all values of ζ, which in general requires (see Eq. (2.7.26)) that

$$\cos\theta = 0. \tag{2.7.30a}$$

For definiteness, we assume that

$$\sin\theta = -1 \tag{2.7.30b}$$

(rather than $+1$). We hence see that the relative phase of the interacting fields is spatially invariant for the case of $\Gamma = 0$. In addition, when $\Gamma = 0$ the coupled-amplitude equations (2.7.22) through (2.7.24) take on the relatively simple forms

$$\frac{du_1}{d\zeta} = -u_1 u_2, \tag{2.7.31}$$

$$\frac{du_2}{d\zeta} = u_1^2. \tag{2.7.32}$$

This second equation can be transformed through use of Eq. (2.7.17) to obtain

$$\frac{du_2}{d\zeta} = 1 - u_2^2, \tag{2.7.33}$$

whose solution is

$$u_2 = \tanh(\zeta + \zeta_0), \tag{2.7.34}$$

where ζ_0 is a constant of integration.

We now assume that the initial conditions are

$$u_1(0) = 1, \qquad u_2(0) = 0. \tag{2.7.35}$$

These conditions imply that no second-harmonic light is incident on the nonlinear crystal, as is the case in most experiments. Then, since $\tanh 0 = 0$, we see that the integration constant ζ_0 is equal to 0 and hence that

$$u_2(\zeta) = \tanh \zeta. \tag{2.7.36}$$

The amplitude u_1 of the fundamental wave is found immediately through use of Eq. (2.7.32) (or through use of Eq. (2.7.17)) to be given by

$$u_1(\zeta) = \operatorname{sech} \zeta. \tag{2.7.37}$$

Recall that $\zeta = z/l$. For the case in which only the fundamental field is present at $z = 0$, the length parameter of Eq. (2.7.19) is given by

$$l = \frac{(n_1 n_2)^{1/2} c}{2\omega_1 d_{\text{eff}} |A_1(0)|}. \tag{2.7.38}$$

The solution given by Eqs. (2.7.36) and (2.7.37) is shown graphically in Fig. 2.7.3. We see that in the limit $\zeta \to \infty$ all of the incident radiation is converted into the second harmonic. In addition, we note that $\tanh(\zeta + \zeta_0)$ has the same asymptotic behavior for any finite value of ζ_0. Thus, whenever Γ is equal to zero, all of the radiation at the fundamental frequency will eventually be converted to the second harmonic, for any initial ratio of u_1 to u_2.

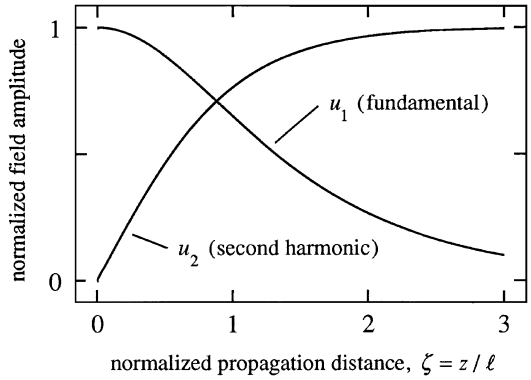

FIGURE 2.7.3: Spatial variations of the fundamental and second-harmonic field amplitudes for the case of perfect phase matching and the boundary condition $u_2(0) = 0$.

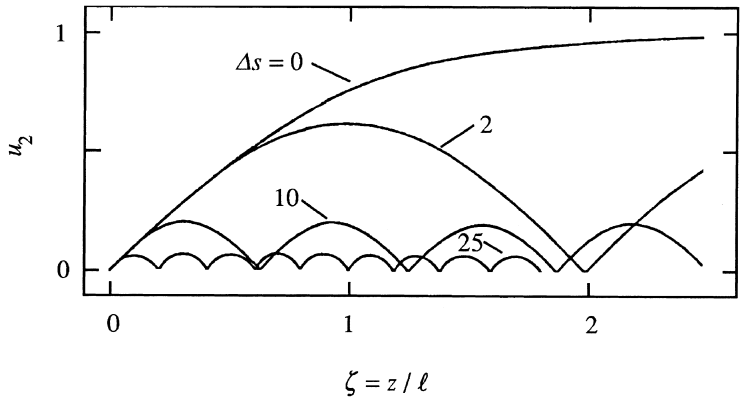

FIGURE 2.7.4: Effect of wavevector mismatch on the efficiency of second-harmonic generation.

As mentioned above, Armstrong et al. have also solved the coupled-amplitude equations describing second-harmonic generation for arbitrary Δk. They find that in this case the solution can also be expressed in terms of elliptic integrals. We shall not reproduce their derivation here; instead we summarize their results graphically in Fig. 2.7.4 for the case in which no radiation is incident at the second-harmonic frequency. We see from the figure that the effect of a nonzero propagation-vector mismatch is to lower the conversion efficiency and to lead to an oscillatory solution.

As an illustration of how to apply the formulas derived in this section, we estimate the conversion efficiency for second-harmonic generation attainable using typical cw lasers. We first estimate the numerical value of the parameter ζ given by Eqs. (2.7.18) and (2.7.38) at the plane $z = L$, where L is the length of the nonlinear crystal. We assume that the incident laser beam carries power P and is focused to a spot size w_0 at the center of the crystal. The field

strength A_1 can then be estimated by the expression

$$I_1 = \frac{P}{\pi w_0^2} = 2n_1 \epsilon_0 c A_1^2. \tag{2.7.39}$$

We assume that the beam is optimally focused in the sense that the focal spot size w_0 is chosen so that the depth b of the focal region is equal to the length L of the crystal, that is,*

$$b \equiv \frac{2\pi w_0^2}{\lambda_1 / n_1} = L, \tag{2.7.40}$$

where λ_1 denotes the wavelength of the incident wave in vacuum. From Eqs. (2.7.39) and (2.7.40), the characteristic value of the laser field amplitude under these conditions is seen to be given by

$$A_1 = \left(\frac{P}{\epsilon_0 c \lambda_1 L} \right)^{1/2}, \tag{2.7.41}$$

and hence the parameter $\zeta = L/l$ is given through use of Eq. (2.7.38) by

$$\zeta = \left(\frac{16\pi^2 d_{\text{eff}}^2 L P}{\epsilon_0 c n_1 n_2 \lambda_1^3} \right)^{1/2}. \tag{2.7.42}$$

Typical values of the parameters appearing in this equation are $d_{\text{eff}} = 4 \times 10^{-12}$ m/V, $L = 0.01$ m, $P = 1$ W, $\lambda = 0.5 \times 10^{-6}$ m, and $n = 2$, which lead to the value $\zeta = 0.14$. The efficiency η for conversion of power from the ω_1 wave to the ω_2 wave can be defined by

$$\eta = \frac{u_2^2(L)}{u_1^2(0)}, \tag{2.7.43}$$

and from Eq. (2.7.36), we see that for the values just given, η is of the order of 2%. However, under optimized conditions, an efficiency as large as 55% has been observed (Chaitanya Kumar et al., 2011).

2.7.1 Applications of Second-Harmonic Generation

Surface Nonlinear Optics

One important application of second-harmonic generation is its use as an exacting diagnostic of the surface properties of optical materials. As noted above, second-harmonic generation is a forbidden process for a material that possesses a center of inversion symmetry. The surface of a material clearly lacks inversion symmetry, and thus second-harmonic generation can occur at

* See also the discussion of nonlinear interactions involving focused Gaussian beams presented in Section 2.10.

the surface of a material of any symmetry group. For the same reason, the intensity and angular distribution of surface second-harmonic generation depends critically on the morphology of a surface and on the presence of impurities on the surface of the material. Good reviews of the early work in this area are given by Shen (1985, 1989), and procedures for calculating the intensity of the second-harmonic light are given by Mizrahi and Sipe (1988a). Second-harmonic generation at a surface is described more fully in Section 2.9.

Nonlinear Optical Microscopy

An important application of harmonic generation is nonlinear microscopy. One motivation for using nonlinear effects and in particular harmonic generation in microscopy is to provide enhanced transverse and longitudinal resolution. Resolution is enhanced because nonlinear processes are excited most efficiently in the region of maximum intensity of a focused laser beam. Microscopy based on harmonic generation also offers the advantage that the signal is far removed in frequency from unwanted background light that results from linear scattering of the incident laser beam. Moreover, light at a wavelength sufficiently long that it will not damage biological materials can be used to achieve a resolution that would normally require a much shorter wavelength. Harmonic-generation microscopy can make use either of the intrinsic nonlinear response of biological materials or can be used with materials that are labeled with nonlinear optical chromophores. Microscopy based on second-harmonic generation in the configuration of a confocal microscope and excited by femtosecond laser pulses was introduced by Curley et al. (1992). Also, harmonic-generation microscopy can be used to form images of transparent (phase) objects, because the phase matching condition of nonlinear optics depends sensitively on the refractive index variation within the sample being imaged (Muller et al., 1998).

Guo et al. (1997) have used tomography based on second-harmonic generation to characterize biological materials. Gauderon et al. (1998) have demonstrated three-dimensional imaging based on second-harmonic generation with fs laser pulses. They used this method to characterize the microcrystal structure of lithium triborate. Campagnola et al. (1999) have used second-harmonic generation to produce images of live cells. Moreaux et al. (2000) have used styrl dyes as labels to image membranes using second-harmonic generation microscopy.

Third-harmonic generation has also been used for imaging applications. Muller et al. (1998) have demonstrated imaging of transparent objects using microscopy based on third-harmonic generation. Yelin and Silberberg (1999) have constructed a scanning microscope based on third-harmonic generation and have used it for the imaging of biological materials.

Nonlinear optical interactions that do not entail harmonic generation also have been shown to hold great promise in optical microscopy. For example, Gustafsson (2005) has shown that through the use of structured illumination and a sample that exhibits saturable absorption, he was able to achieve a transverse resolution of 50 nm. Moreover, Westphal and Hell (2005) have

shown the depletion of fluorescence by means of stimulated emission can be used to achieve extremely high subwavelength resolution (in particular, 16 nm or 1/50 of their operating wavelength) in optical microscopy.

2.8 Difference-Frequency Generation and Parametric Amplification

Let us now consider the situation shown in Fig. 2.8.1, in which optical waves at frequencies ω_3 and ω_1 interact in a lossless nonlinear optical medium to produce an output wave at the difference frequency $\omega_2 = \omega_3 - \omega_1$. For simplicity, we assume that the ω_3 wave is a strong wave (i.e., is undepleted by the nonlinear interaction, so that we can treat A_3 as being essentially constant), and for the present we assume that no field is incident on the medium at frequency ω_2.

The coupled-amplitude equations describing this interaction are obtained by a method analogous to that used in Section 2.2 to obtain the equations describing sum-frequency generation and have the form

$$\frac{dA_1}{dz} = \frac{2id_{\text{eff}}\omega_1^2}{k_1c^2}A_3A_2^*e^{i\Delta kz}, \tag{2.8.1a}$$

$$\frac{dA_2}{dz} = \frac{2id_{\text{eff}}\omega_2^2}{k_2c^2}A_3A_1^*e^{i\Delta kz}, \tag{2.8.1b}$$

where

$$\Delta k = k_3 - k_1 - k_2. \tag{2.8.2}$$

We first solve these equations for the case of perfect phase matching—that is, $\Delta k = 0$. We differentiate Eq. (2.8.1b) with respect to z and introduce the complex conjugate of Eq. (2.8.1a) to eliminate dA_1^*/dz from the right-hand side. We thereby obtain the equation

$$\frac{d^2A_2}{dz^2} = \frac{4d_{\text{eff}}^2\omega_1^2\omega_2^2}{k_1k_2c^4}A_3A_3^*A_2 \equiv \kappa^2A_2, \tag{2.8.3}$$

where we have introduced the real coupling constant κ given by

$$\kappa^2 = \frac{4d_{\text{eff}}^2\omega_1^2\omega_2^2}{k_1k_2c^4}|A_3|^2. \tag{2.8.4}$$

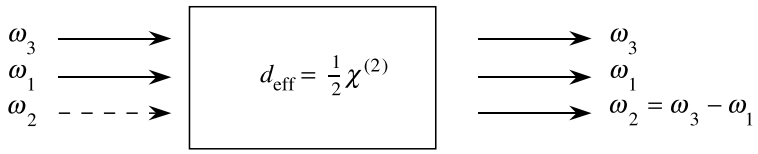

FIGURE 2.8.1: Difference-frequency generation. Typically, no input field is applied at frequency ω_2.

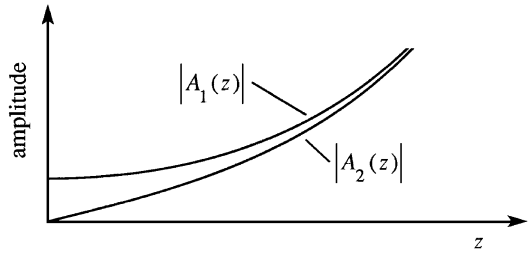

FIGURE 2.8.2: Spatial evolution of A_1 and A_2 for difference-frequency generation for the case $\Delta k = 0$ in the constant-pump approximation.

The general solution to this equation is

$$A_2(z) = C \sinh \kappa z + D \cosh \kappa z, \tag{2.8.5}$$

where C and D are integration constants whose values depend on the initial conditions.

We now assume the initial conditions

$$A_2(0) = 0, \qquad A_1(0) \text{ arbitrary}. \tag{2.8.6}$$

The solution to Eqs. (2.8.1a) and (2.8.1b) that meets these initial conditions is readily found to be

$$A_1(z) = A_1(0) \cosh \kappa z, \tag{2.8.7}$$

$$A_2(z) = i\left(\frac{n_1\omega_2}{n_2\omega_1}\right)^{1/2} \frac{A_3}{|A_3|} A_1^*(0) \sinh \kappa z. \tag{2.8.8}$$

The nature of this solution is shown in Fig. 2.8.2. Note that both the ω_1 and the ω_2 fields experience monotonic growth and that asymptotically each field experiences exponential growth (i.e., for $\kappa z \gg 1$, each grows as $e^{\kappa z}$). We see from the form of the solution that the ω_1 field retains its initial phase and is simply amplified by the interaction, whereas the generated wave at frequency ω_2 has a phase that depends both on that of the pump wave and on that of the ω_1 wave. This behavior of monotonic growth of both waves is qualitatively dissimilar from that of sum-frequency generation, where oscillatory behavior occurs.

The reason for the different behavior in this case can be understood intuitively in terms of the energy-level diagram shown in Fig. 2.8.3. We can think of diagram (a) as showing how the presence of a field at frequency ω_1 stimulates the downward transition that leads to the generation of the ω_2 field. Likewise, diagram (b) shows that the ω_2 field stimulates the generation of the ω_1 field. Hence the generation of the ω_1 field reinforces the generation of the ω_2 field, and vice versa, leading to the exponential growth of each wave.

Since the ω_1 field is amplified by the process of difference-frequency generation, which is a parametric process, this process is also known as parametric amplification. In this language,

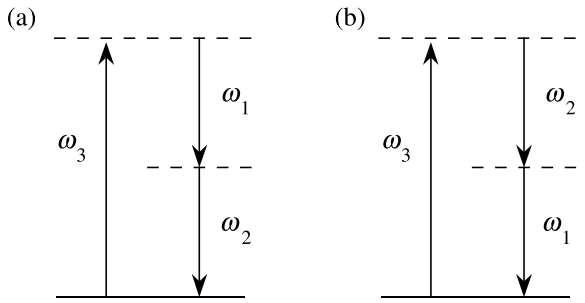

FIGURE 2.8.3: Illustration of how the generation of light at frequency ω_2 reinforces the generation of light at frequency ω_1 and vice versa.

one says that the signal wave (the ω_1 wave) is amplified by the nonlinear mixing process, and an idler wave (at $\omega_2 = \omega_3 - \omega_1$) is generated by the process. If mirrors that are highly reflecting at frequencies ω_1 and/or ω_2 are placed on either side of the nonlinear medium to form an optical resonator, oscillation can occur as a consequence of the gain of the parametric amplification process. Such a device is known as a parametric oscillator and is described in greater detail in the following section. The first cw optical parametric oscillator was built by Giordmaine and Miller (1965, 1966). The theory of parametric amplification and parametric oscillators has been reviewed by Byer and Herbst (1977).

The solution to the coupled-amplitude equations (2.8.1) for the general case of arbitrary $\Delta k \neq 0$ makes a good exercise for the reader (see Problem 4 at the end of this chapter).

2.9 Optical Parametric Oscillators

We noted in the previous section that the process of difference-frequency generation necessarily leads to the amplification of the lower-frequency input field. This amplification process is known as optical parametric amplification, and the gain resulting from this process can be used to construct a device known as an optical parametric oscillator (OPO). These features are summarized in Fig. 2.9.1. Here we adopt the standard notation (see part (a) of the figure) that the highest-frequency wave is known as the pump wave and the lower-frequency waves are known as the signal and idler waves. There is no consistent usage regarding the naming of the signal and idler waves. However, the desired output wave is typically referred to as the signal wave. The gain associated with the process of optical parametric amplification can in the presence of feedback produce oscillation, as shown in part (b) of the figure. If the end mirrors of this device are highly reflecting at both frequencies ω_s and ω_i, the device is known as a doubly resonant oscillator; if they are highly reflecting at ω_s or ω_i but not at both, the device is known as a singly resonant oscillator. Note that when an OPO is operated near the point of degeneracy

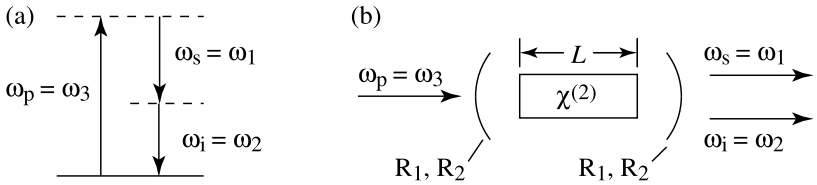

FIGURE 2.9.1: (a) Relationship between difference-frequency generation and optical parametric amplification. (b) The gain associated with the process of optical parametric amplification can be used to construct the device shown, which is known as an optical parametric oscillator.

($\omega_s = \omega_i$) it tends to operate as a doubly resonant oscillator.* The optical parametric oscillator has proven to be a versatile source of frequency-tunable radiation throughout the infrared, visible, and ultraviolet spectral regions. It can produce either a continuous-wave output or pulses of nanosecond, picosecond, or femtosecond duration.

Let us recall the treatment of Section 2.8 on how to calculate the gain of the process of optical parametric amplification. For convenience, we label the pump, signal, and idler frequencies as $\omega_p = \omega_3$, $\omega_s = \omega_1$, and $\omega_i = \omega_2$. We take the coupled-amplitude equations to have the form (see also Eqs. (2.8.1))

$$\frac{dA_1}{dz} = \frac{2i\omega_1^2 d_{\text{eff}}}{k_1 c^2} A_3 A_2^* e^{i\Delta kz}, \tag{2.9.1a}$$

$$\frac{dA_2}{dz} = \frac{2i\omega_2^2 d_{\text{eff}}}{k_2 c^2} A_3 A_1^* e^{i\Delta kz}, \tag{2.9.1b}$$

where $\Delta k \equiv k_3 - k_1 - k_2$. These equations possess the solution (see Problem 4 at the end of this chapter)

$$A_1(z) = \left[A_1(0)\left(\cosh gz - \frac{i\Delta k}{2g}\sinh gz\right) + \frac{\kappa_1}{g}A_2^*(0)\sinh gz\right]e^{i\Delta kz/2}, \tag{2.9.2a}$$

$$A_2(z) = \left[A_2(0)\left(\cosh gz - \frac{i\Delta k}{2g}\sinh gz\right) + \frac{\kappa_2}{g}A_1^*(0)\sinh gz\right]e^{i\Delta kz/2}, \tag{2.9.2b}$$

where we have introduced the quantities

$$g = \left[\kappa_1\kappa_2^* - (\Delta k/2)^2\right]^{1/2} \quad \text{and} \quad \kappa_i = \frac{2i\omega_i^2 d_{\text{eff}} A_3}{k_i c^2}. \tag{2.9.3}$$

For the special case of perfect phase matching ($\Delta k = 0$) and under the assumption that the input amplitude of field A_2 vanishes ($A_2(0) = 0$), the solution reduces to

$$A_1(z) = A_1(0)\cosh gz \Rightarrow \tfrac{1}{2}A_1(0)\exp(gz) \tag{2.9.4a}$$

* In principle, polarization effects can be used to suppress cavity feedback for either the signal or idler wave for the case of type-II phase matching.

$$A_2(z) = i\left(\frac{n_1\omega_2}{n_2\omega_1}\right)^{1/2}\frac{A_3}{|A_3|}A_1^*(0)\sinh gz \Rightarrow O(1)A_1^*(0)\exp(gz). \tag{2.9.4b}$$

In each expression, the last form gives the asymptotic value for large z, and the symbol $O(1)$ means of the order of unity. One sees that asymptotically both waves experience exponential growth, with an amplitude gain coefficient of g.

Threshold for Parametric Oscillation

We next consider the threshold condition for the establishment of parametric oscillation. We treat the device shown in Fig. 2.9.1(b), in which the two end mirrors are assumed to be identical but are allowed to have different (intensity) reflectivities R_1 and R_2 at the signal and idler frequencies.

We first present a simple model of the threshold condition by taking it to be a statement that the fractional energy gain per pass must equal the fractional energy loss per pass. Under the assumptions of exact cavity resonance, of perfect phase matching ($\Delta k = 0$), and that the cavity is doubly resonant with the same reflectivity at the signal and idler frequencies (that is, $R_1 = R_2 \equiv R$, $(1 - R) \ll 1$), this condition can be expressed as

$$\left(e^{2gL} - 1\right) = 2(1 - R). \tag{2.9.5}$$

Under the realistic condition that the single-pass exponential gain $2gL$ is not large compared to unity, this condition becomes

$$gL = 1 - R. \tag{2.9.6}$$

This is the threshold condition formulated by Giordmaine and Miller (1965, 1966).

The threshold condition for optical parametric oscillation can be formulated more formally as a statement that the fields within the resonator must replicate themselves each round trip. For arbitrary end-mirror reflectivities at the signal and idler frequencies, this condition can be expressed, again assuming perfect phase matching, as

$$A_1(0) = \left[A_1(0)\cosh gL + \frac{\kappa_1}{g}A_2^*(0)\sinh gL\right](1 - l_1), \tag{2.9.7a}$$

$$A_2^*(0) = \left[A_2^*(0)\cosh gL + \frac{\kappa_2^*}{g}A_1(0)\sinh gL\right](1 - l_2), \tag{2.9.7b}$$

where $l_i = 1 - R_i e^{-\alpha_i L}$ is the fractional amplitude loss per pass, α_i being the absorption coefficient of the crystal at frequency $\omega_{\rm i}$. By requiring that both of Eqs. (2.9.7) be satisfied simultaneously, we find the threshold condition to be

$$\cosh gL = 1 + \frac{l_1 l_2}{2 - l_1 - l_2}. \tag{2.9.8}$$

The threshold conditions for both doubly resonant oscillators and singly resonant oscillators are contained in this result. The doubly resonant oscillator is described by taking the limit of low loss for both the signal and idler waves ($l_1,\ l_2 \ll 1$). In this limit, $\cosh gL$ can be approximated by $1 + \frac{1}{2}\ g^2L^2$, leading to the conclusion that the threshold condition for a doubly resonant oscillator is

$$g^2L^2 = l_1 l_2, \tag{2.9.9}$$

in consistency with Eq. (2.9.6).

The threshold condition for a singly resonant oscillator can be obtained by assuming that there is no feedback for the idler frequency, that is, that $l_2 = 1$. If we assume low loss for the signal frequency (that is, $l_1 \ll 1$), the threshold condition becomes

$$g^2L^2 = 2l_1. \tag{2.9.10}$$

Note that the threshold value of gL for a singly resonant oscillator is larger than that of the doubly resonant oscillator by a factor of $(2/l_2)^{1/2}$. Despite this fact, it is usually desirable to configure optical parametric oscillators to be singly resonant because of the increased stability of singly resonant oscillators, for reasons that are explained below.

For simplicity, the treatment of this subsection has assumed the case of perfect phase matching. It is straightforward to show that the threshold condition for the case $\Delta k \neq 0$ can be obtained by replacing g^2 by $g^2\,\mathrm{sinc}^2(\Delta kL/2)$ in Eqs. (2.9.9) and (2.9.10).

Wavelength Tuning of an OPO

The condition of energy conservation $\omega_s + \omega_i = \omega_p$ allows any frequency ω_s smaller than ω_p to be generated by an optical parametric oscillator. The output frequency ω_s can be controlled through the phase-matching condition $\Delta k = 0$, which invariably can be satisfied for at most one pair of frequencies ω_s and ω_i. The output frequency bandwidth can often be narrowed by placing wavelength-selective items (such as etalons) inside the OPO cavity.

The principles of phase matching were described earlier in Section 2.3. Recall that phase matching can be achieved either by varying the orientation of the nonlinear crystal (angle phase matching) or by varying the temperature of the crystal.

2.9.1 Influence of Cavity Mode Structure on OPO Tuning

Let us now take a more detailed look at the tuning characteristics of an OPO. We shall see that both the tuning and stability characteristics of an OPO are very different for the singly resonant and doubly resonant cases.

Note first that under typical conditions the cavity mode spacing and cavity resonance width tend to be much smaller than the width of the gain curve of the optical parametric amplification

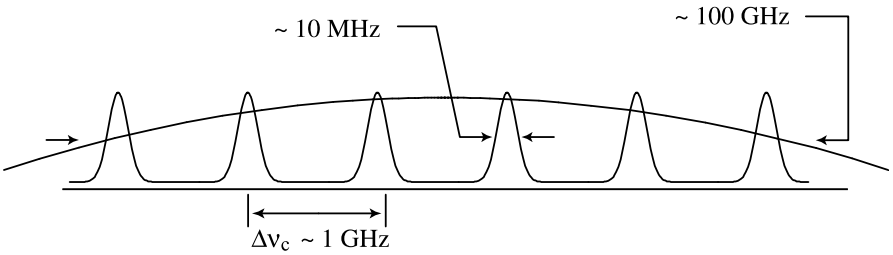

FIGURE 2.9.2: Schematic representation of the gain spectrum (the broad curve) and cavity mode structure of an OPO. Note that typically many cavity modes lie beneath the gain profile of the OPO.

process. This circumstance is illustrated in Fig. 2.9.2.* Let us next consider which of these cavity modes will actually undergo oscillation.

For the case of a singly resonant oscillator (displayed in part (a) of Fig. 2.9.3), the situation is relatively simple. Oscillation occurs on the cavity mode closest to the peak of the gain curve. Note also that (barring mechanical instabilities, etc.) oscillation will occur on only one cavity mode. The reason for this behavior is that once oscillation commences on the cavity mode closest to the peak of the gain curve, the pump power becomes depleted, thus lowering the gain to the value of the loss for this mode. By assumption, the gain will be smaller at the frequencies of the other cavity modes, and thus these modes will be below threshold for oscillation. This behavior is very much analogous to that of a homogeneously broadened laser, which tends to oscillate on a single cavity mode.

Consider now the different situation of a doubly resonant oscillator (Fig. 2.9.3(b)). For a doubly resonant oscillator, oscillation is very much favored under conditions such that a signal and its corresponding idler mode can simultaneously support oscillation. Note from the figure that neither of these modes is necessarily the mode closest to the peak of the gain curve (which occurs at $\Delta k = 0$). As a consequence doubly resonant oscillators tend not to tune smoothly. Moreover, such devices tend not to run stably, because, for example, small fluctuations in the pump frequency or the cavity length L can lead to disproportionately large variations in the signal frequency.

The argument just presented, based on the structure of Fig. 2.9.3(b), presupposes that the cavity modes are not equally spaced. In fact, it is easy to show that the cavity mode spacing for

* This example assumes that the cavity length L_c is 15 cm so that the cavity mode spacing $\Delta\nu_c = c/2L_c$ is 1 GHz, that the cavity finesse $\mathcal{F}$ is 100 so that the linewidth associated with each mode is 1 GHz/$\mathcal{F}$ = 10 MHz and that the width of the gain curve is 100 GHz. This gain linewidth is estimated by assuming that ΔkL (which is zero at the center of the gain line and where L is the crystal length) drops to the value π at the edge of the gain line. If we then assume that Δk changes with signal frequency because of material dispersion, and that $dn/d\nu$ is of the order of 10^{-15} sec, we obtain 100 GHz as the gain bandwidth.

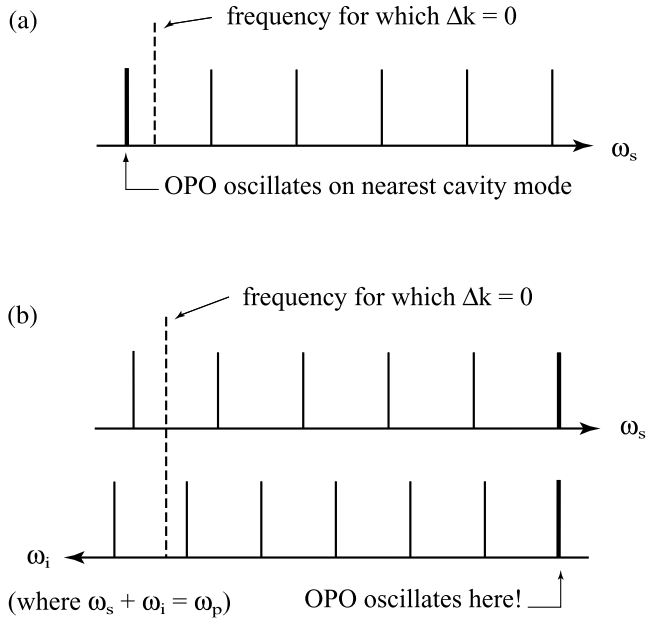

FIGURE 2.9.3: (a) Symbolic representation of the mode structure of a singly resonant OPO. (b) Symbolic representation of the mode structure of a doubly resonant OPO. The signal-frequency and idler-frequency axes increase in opposite directions, such that at each horizontal point $\omega_s + \omega_i$ has the fixed value ω_p. Thus, any point on the axis represents a point where the energy conservation relation $\omega_s + \omega_i = \omega_p$ is satisfied, although only at points where signal and idler modes occur at the same horizontal point is the double-resonance condition satisfied.

a cavity of length L_c filled with a dispersive medium is given by

$$\Delta\nu_c = \frac{1}{n^{(g)}}\frac{c}{2L_c}; \quad \text{where } n^{(g)} = n + \nu\,\frac{dn}{d\nu} \tag{2.9.11}$$

(see Problems 7 and 8 at the end of this chapter), which normally is not constant as a function of frequency ν. Here $n^{(g)}$ is known as the group index.

Let us next examine more quantitatively the nature of the decreased stability of the doubly resonant oscillator. We first estimate the characteristic frequency separation $\delta\omega$ between the peak of the gain curve and the frequency of actual oscillation, which is illustrated pictorially in Fig. 2.9.3(b). To do so, it is convenient to first introduce the quantity

$$\Delta\omega \equiv \omega_p - \omega_s^{(m)} - \omega_i^{(m)}, \tag{2.9.12}$$

where $\omega_s^{(m)}$ is one of the signal cavity-mode frequencies and similarly for $\omega_i^{(m)}$. Clearly, oscillation can occur only for a pair of modes such that $\Delta\omega \approx 0$ (or more precisely where $\Delta\omega \lesssim \delta\omega_c$ where $\delta\omega_c$ is the spectral width of the cavity resonance). Note next that in jumping by one

cavity mode for both ω_s and ω_i, the quantity $\Delta\omega$ will change by the amount

$$\delta(\Delta\omega) = 2\pi\left(\frac{c}{2n_s^{(g)}L_c} - \frac{c}{2n_i^{(g)}L_c}\right) = \frac{\pi c}{L_c}\left(\frac{n_i^{(g)} - n_s^{(g)}}{n_s^{(g)}n_i^{(g)}}\right). \tag{2.9.13}$$

We next estimate the value of the frequency separation $\delta\omega$ by noting that it corresponds to a change in $\Delta\omega$ from its value near the point $\Delta k = 0$ to its value (≈ 0) at the oscillation point. Unless the length of the OPO cavity is actively controlled, the value of $\Delta\omega$ near $\Delta k = 0$ can be as large as one-half of a typical mode spacing or

$$\Delta\omega_0 \simeq \frac{1}{2}\left(\frac{2\pi c}{2n^{(g)}L_c}\right) = \frac{\pi c}{2n^{(g)}L_c}, \tag{2.9.14}$$

where $n^{(g)}$ is some typical value of the group index. The number of modes between the peak of the gain curve and the actual operating point under this situation is thus of the order of

$$N = \frac{\Delta\omega_0}{\delta(\Delta\omega)} = \frac{n^{(g)}}{2(n_s^{(g)} - n_i^{(g)})} \tag{2.9.15}$$

and the characteristic frequency separation $\delta\omega$ is thus given by

$$\delta\omega = \Delta\omega_c N \simeq \frac{2\pi c}{2n^{(g)}L_c}N = \frac{\pi c}{2L_c}\frac{1}{(n_s^{(g)} - n_i^{(g)})}. \tag{2.9.16}$$

Note that this shift can be very large for $n_s^{(g)} \approx n_i^{(g)}$.

The model just presented can be used to estimate an important quantity, the operational linewidth $\delta\omega^{(\mathrm{OPO})}$ of the oscillator. We noted above that in principle an OPO should oscillate on a single cavity mode. However, because of unavoidable technical noise, an OPO might be expected to oscillate (simultaneously or sequentially) on several different cavity modes. The technical noise might be in the form of mechanical vibrations of the OPO cavity, leading to a jitter of amount $\delta\omega_c$ in the resonance frequency of each cavity mode. Alternatively, the technical noise might be in the form of the spectral breadth $\delta\omega_\mathrm{p}$ of the pump radiation. Whichever effect is larger might be expected to dominate, and thus the effective value of the technical noise is given by $\delta\omega_\mathrm{eff} = \max(\delta\omega_c, \delta\omega_\mathrm{p})$. Analogously to Eq. (2.9.15), one then expects the number of modes that undergo oscillation to be given by

$$N_\mathrm{osc} = \frac{\delta\omega_\mathrm{eff}}{\delta(\Delta\omega)} = \frac{\max(\delta\omega_\mathrm{p}, \delta\omega_c)}{\delta(\Delta\omega)}. \tag{2.9.17}$$

Consequently, the OPO linewidth is expected to be

$$\delta\omega^{(\mathrm{osc})} = N_\mathrm{OPO}\Delta\omega_c = \frac{n_g}{n_g^{(s)} - n_g^{(i)}}\max(\delta\omega_\mathrm{p}, \delta\omega_c). \tag{2.9.18}$$

Note that the linewidth of an OPO tends to be much greater than that of the pump field or that of the bare OPO cavity. Active stabilization can be used to decrease this linewidth.

Equation (2.9.18) has important implications in the design of OPOs. Note that this expression formally diverges at the point of degeneracy for a type-I (but not a type-II) OPO. The narrower linewidth of a type-II OPO compared to that of a type-I OPO constructed of the same material has been observed in practice by Bosenberg and Tang (1990).

We conclude this section with a brief historical summary of progress in the development of OPOs. As mentioned above, the first operating OPO was demonstrated by Giordmaine and Miller (1965, 1966); it utilized the nonlinear optical response of lithium niobate and worked in the pulsed regime. Continuous-wave operation of an OPO was demonstrated by Smith et al. (1968) and utilized a $Ba_2NaNb_5O_{15}$ nonlinear crystal. Interest in the development of OPOs was renewed in the 1980s as a consequence of the availability of new nonlinear materials such as β-BaB_2O_4 (beta-barium borate or BBO), LiB_3O_5 (lithium borate or LBO), and $KTiOPO_4$ (KTP), which possess high nonlinearity, high resistance to laser damage, and large birefringence. These materials led to the rapid development of new OPO capabilities, such as continuous tunability from 0.42 to 2.3 μm in a BBO OPO with conversion efficiencies as large as 32% (Bosenberg et al., 1989), and OPOs that can produce tunable femtosecond pulses in KTP Edelstein et al., 1989. The use of quasi-phase-matching in periodically poled lithium niobate has also been utilized to produce novel OPOs. For additional information, the reader might refer to Byer et al. (1973), Simon and Tittel (1994), and Ebrahimzadeh and Dunn (2001).

2.10 Nonlinear Optical Interactions with Focused Gaussian Beams

In the past several sections we have treated nonlinear optical interactions in the approximation in which the interacting waves are taken to be infinite plane waves. However, in practice, the incident radiation is usually focused into the nonlinear optical medium in order to increase its intensity and thereby increase the efficiency of the nonlinear optical process. The present section explores the nature of nonlinear optical interactions that are excited by focused laser beams.

2.10.1 Paraxial Wave Equation

We begin by deriving what is known as the paraxial wave equation. We assume that each frequency component of the beam obeys a wave equation of the form of Eq. (2.1.21)—that is,

$$\nabla^2 \tilde{\mathbf{E}}_n - \frac{1}{(c/n)^2}\frac{\partial^2 \tilde{\mathbf{E}}_n}{\partial t^2} = \frac{1}{\epsilon_0 c^2}\frac{\partial^2 \tilde{\mathbf{P}}_n}{\partial t^2}. \tag{2.10.1}$$

We next represent the electric field $\tilde{\mathbf{E}}_n$ and polarization $\tilde{\mathbf{P}}_n$ as

$$\tilde{\mathbf{E}}_n(\mathbf{r}, t) = \mathbf{A}_n(\mathbf{r}) e^{i(k_n z - \omega_n t)} + \text{c.c.}, \tag{2.10.2a}$$

$$\tilde{\mathbf{P}}_n(\mathbf{r},t) = \mathbf{p}_n(\mathbf{r})e^{i(k_n' z-\omega_n t)} + \text{c.c.} \tag{2.10.2b}$$

Here we allow $\tilde{\mathbf{E}}_n$ and $\tilde{\mathbf{P}}_n$ to represent nonplane waves by allowing the complex amplitudes $\mathbf{A}_n$ and $\mathbf{p}_n$ to be spatially varying quantities. In addition, we allow the possibility of a wavevector mismatch by allowing the wavevector of $\tilde{\mathbf{P}}_n$ to be different from that of $\tilde{\mathbf{E}}_n$. We next substitute Eqs. (2.10.2) into (2.10.1). Since we have specified the z direction as the dominant direction of propagation of the wave $\tilde{\mathbf{E}}_n$, it is useful to express the Laplace operator as $\nabla^2 = \partial^2/\partial z^2 + \nabla_{\mathrm{T}}^2$, where the transverse Laplacian is given by $\nabla_{\mathrm{T}}^2 = \partial^2/\partial x^2 + \partial^2/\partial y^2$ in rectangular coordinates and is given by $\nabla_{\mathrm{T}}^2 = (1/r)(\partial/\partial r)(r\partial/\partial r) + (1/r)^2\partial^2/\partial\phi^2$, where $r^2 = x^2 + y^2$, in cylindrical coordinates. As in the derivation of Eq. (2.2.10), we now make the slowly varying amplitude approximation, that is, we assume that any longitudinal variation of $\mathbf{A}_n$ can occur only over distances much larger than an optical wavelength. We hence find that Eq. (2.10.1) becomes

$$2ik_n\frac{\partial \mathbf{A}_n}{\partial z} + \nabla_{\mathrm{T}}^2\mathbf{A}_n = -\frac{\omega_n^2}{\epsilon_0 c^2}\mathbf{p}_n e^{i\Delta k z}, \tag{2.10.3}$$

where $\Delta k = k_n' - k_n$. This result is known as the paraxial wave equation, because the approximation of neglecting the contribution $\partial^2 A/\partial z^2$ on the left-hand side is justifiable insofar as the wave $\mathbf{E}_n$ is propagating primarily along the z axis.

2.10.2 Gaussian Beams

Let us first study the nature of the solution to Eq. (2.10.3) for the case of the free propagation of an optical wave, that is, for the case in which the source term containing $\mathbf{p}_n$ vanishes. The paraxial wave equation is solved in such a case by a beam having a transverse intensity distribution that is everywhere a Gaussian and that can be represented in the scalar approximation as (Kogelnik and Li, 1966)

$$A(r,z) = \mathcal{A}\frac{w_0}{w(z)}e^{-r^2/w(z)^2}e^{ikr^2/2R(z)}e^{i\Phi(z)}, \tag{2.10.4a}$$

where

$$w(z) = w_0\left[1 + \left(\lambda z/\pi w_0^2\right)^2\right]^{1/2} \tag{2.10.4b}$$

represents the $1/e$ radius of the field distribution, where

$$R(z) = z\left[1 + \left(\pi w_0^2/\lambda z\right)^2\right] \tag{2.10.4c}$$

represents the radius of curvature of the optical wavefront, and where

$$\Phi(z) = -\arctan\left(\lambda z/\pi w_0^2\right) \tag{2.10.4d}$$

represents the spatial variation of the phase of the wave (measured with respect to that of an infinite plane wave). In these formulas, w_0 represents the beam waist radius (that is, the value of w at the plane $z = 0$), and $\lambda = 2\pi c/n\omega$ represents the wavelength of the radiation in the medium. The angular divergence of the beam in the far field is given by $\theta_{\text{ff}} = \lambda/\pi w_0$. The nature of this solution is illustrated in Fig. 2.10.1.

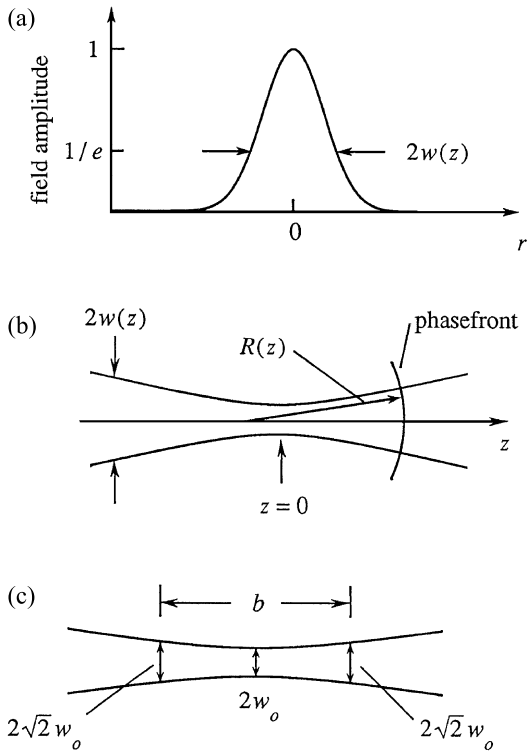

FIGURE 2.10.1: (a) Field amplitude distribution of a Gaussian laser beam. (b) Variation of the beam radius w and wavefront radius of curvature R with position z. (c) Relation between the beam waist radius and the confocal parameter b.

For theoretical work it is often convenient to represent the Gaussian beam in the more compact (but less intuitive) form (see Problem 10 at the end of the chapter)

$$A(r, z) = \frac{\mathcal{A}}{1 + i\zeta} e^{-r^2/w_0^2(1+i\zeta)}. \tag{2.10.5a}$$

Here*

$$\zeta = 2z/b \tag{2.10.5b}$$

* Note that the quantity ζ defined here bears no relation to the quantity ζ introduced in Eq. (2.7.18) in our discussion of second-harmonic generation.

is a dimensionless longitudinal coordinate defined in terms of the confocal parameter

$$b = 2\pi w_0^2/\lambda = k w_0^2, \tag{2.10.5c}$$

which, as illustrated in part (c) of Fig. 2.10.1, is a measure of the longitudinal extent of the focal region of the Gaussian beam. It is worth noting that the confocal parameter b is related to another standard quantity known as the Rayleigh range z_R through the relation $b = 2z_R$. The total power $\mathcal{P}$ carried by a Gaussian laser beam can be calculated by integrating over the transverse intensity distribution of the beam. Since $\mathcal{P} = \int I(r) 2\pi r dr$, where the intensity is given by $I = 2n\epsilon_0 c|A|^2$, we find that

$$\mathcal{P} = n\epsilon_0 c\pi w_0^2 |\mathcal{A}|^2. \tag{2.10.6}$$

2.10.3 Harmonic Generation Using Focused Gaussian Beams

Let us now treat harmonic generation excited by a fundamental beam of frequency ω and a Gaussian transverse profile. For generality, we consider the generation of the qth harmonic.* According to Eq. (2.10.3), the amplitude A_q of the q-th harmonic (that is, the $\omega_q = q\omega$ frequency component) of the optical field must obey the equation

$$2ik_q \frac{\partial A_q}{\partial z} + \nabla_T^2 A_q = -\frac{\omega_q^2}{c^2} \chi^{(q)} A_1^q e^{i\Delta k z}, \tag{2.10.7}$$

where $\Delta k = qk_1 - k_q$ and where we have set the complex amplitude p_q of the nonlinear polarization equal to $p_q = \epsilon_0 \chi^{(q)} A_1^q$. Here $\chi^{(q)}$ is the nonlinear susceptibility describing qth-harmonic generation—that is, $\chi^{(q)} = \chi^{(q)}(q\omega = \omega + \omega + \cdots + \omega)$, and A_1 is the complex amplitude of the fundamental wave, which according to Eq. (2.10.5a) can be represented as

$$A_1(r, z) = \frac{\mathcal{A}_1}{1 + i\zeta} e^{-r^2/w_0^2(1+i\zeta)}. \tag{2.10.8}$$

We work in the constant-pump approximation. We solve Eq. (2.10.7) by adopting the trial solution

$$A_q(r, z) = \frac{\mathcal{A}_q(z)}{1 + i\zeta} e^{-qr^2/w_0^2(1+i\zeta)}, \tag{2.10.9}$$

where $\mathcal{A}_q(z)$ is a function of z. One might guess this form for the trial solution because its radial dependence is identical to that of the source term in Eq. (2.10.7). Note also that (ignoring

* Our current treatment is valid for both even and odd values of q, even though the nonlinear susceptibility $\chi^{(q)}$ would normally be expected to vanish for even values of q for noncentrosymmetric media of the sort implicitly assumed here.

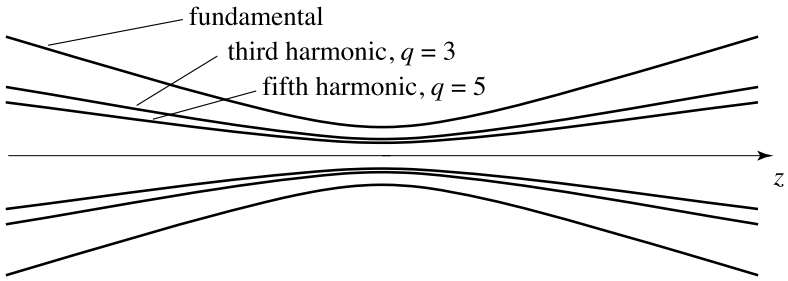

FIGURE 2.10.2: Variation of the beam parameter $w(z)$ in the focal region for the fundamental and third- and fifth-harmonic beams. All three fields have the same confocal parameter b, although the beam waist radius w_0 and far field diffraction angle scale as $q^{-1/2}$.

the longitudinal variation of $\mathcal{A}_q(z)$) the trial solution corresponds to a beam with the same confocal parameter as the fundamental beam Eq. (2.10.8); this behavior makes sense in that the harmonic wave is generated coherently over a region whose longitudinal extent is equal to that of the fundamental wave. If the trial solution Eq. (2.10.9) is substituted into Eq. (2.10.7), we find that it satisfies this equation so long as $\mathcal{A}_q(z)$ obeys the (ordinary) differential equation

$$\frac{d\mathcal{A}_q}{dz} = \frac{iq\omega}{2n_q c}\chi^{(q)}\mathcal{A}_1^q \frac{e^{i\Delta kz}}{(1+i\zeta)^{q-1}}. \tag{2.10.10}$$

This equation can be integrated directly to obtain

$$\mathcal{A}_q(z) = \frac{iq\omega}{2nc}\chi^{(q)}\mathcal{A}_1^q J_q(\Delta k, z_0, z), \tag{2.10.11a}$$

where

$$J_q(\Delta k, z_0, z) = \int_{z_0}^{z} \frac{e^{i\Delta kz'}\,dz'}{(1+2iz'/b)^{q-1}}, \tag{2.10.11b}$$

and where z_0 represents the value of z at the entrance to the nonlinear medium. We see that the harmonic radiation is generated with a confocal parameter equal to that of the incident laser beam, as shown in Fig. 2.10.2. Hence the beam waist radius of the qth harmonic radiation is $q^{1/2}$ times smaller than that of the incident beam, and the far-field diffraction angle $\theta_{\text{ff}} = \lambda/\pi w_0$ is $q^{1/2}$ times smaller than that of the incident laser beam. We have solved Eq. (2.10.7) by guessing the correct form (Eq. (2.10.9)) for the trial solution; a constructive solution to Eq. (2.10.7) has been presented by Kleinman et al. (1966) for second-harmonic generation and by Ward and New (1969) for the general case of qth-harmonic generation.

The integral appearing in Eq. (2.10.11b) can be evaluated analytically for certain special cases. One such case is the plane-wave limit, where $b \gg |z_0|, |z|$. In this limit the integral

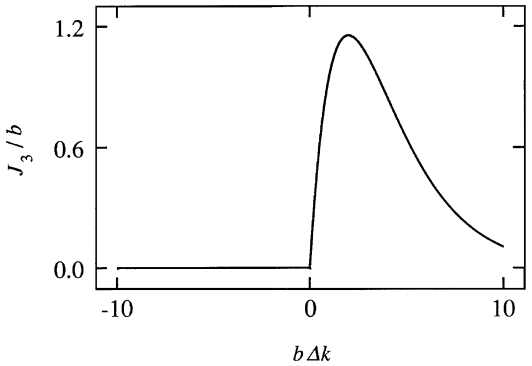

FIGURE 2.10.3: Dependence of the phase-matching factor J_3 for third-harmonic generation on the normalized confocal parameter $b\Delta k$, in the tight-focusing limit.

reduces to

$$J_q(\Delta k, z_0, z) = \int_{z_0}^{z} e^{i\Delta k z'}\, dz' = \frac{e^{i\Delta k z} - e^{i\Delta k z_0}}{i\Delta k}, \tag{2.10.12a}$$

which implies that

$$\left|J_q(\Delta k, z_0, z)\right|^2 = L^2 \operatorname{sinc}^2\left(\frac{\Delta k L}{2}\right) \tag{2.10.12b}$$

where $L = z - z_0$ is the length of the interaction region.

The opposite limiting case is that in which the fundamental wave is focused tightly within the interior of the nonlinear medium; this condition implies that $z_0 = -|z_0|$, $z = |z|$, and $b \ll |z_0|, |z|$. In this limit the integral in Eq. (2.10.11b) can be approximated by replacing the limits of integration by plus and minus infinity—that is,

$$J_q(\Delta k, z_0, z) = \int_{-\infty}^{\infty} \frac{e^{i\Delta k z'}\, dz'}{(1 + 2iz'/b)^{q-1}}. \tag{2.10.13a}$$

This integral can be evaluated by means of a straightforward contour integration. One finds that

$$J_q(\Delta k, z_0, z) = \begin{cases} 0, & \Delta k \le 0, \\ \frac{b}{2}\,\frac{2\pi}{(q-2)!}\left(\frac{b\Delta k}{2}\right)^{q-2} e^{-b\Delta k/2}, & \Delta k > 0. \end{cases} \tag{2.10.13b}$$

This functional form is illustrated for the case of third-harmonic generation ($q = 3$) in Fig. 2.10.3. We find the somewhat surprising result that the efficiency of third-harmonic generation in the tight-focusing limit vanishes identically for the case of perfect phase matching ($\Delta k = 0$) and is maximized through the use of a positive wavevector mismatch. This behavior can be understood in terms of the phase shift of π radians that any beam of light experiences

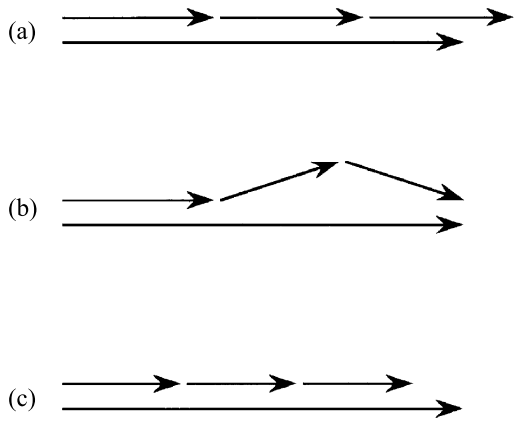

FIGURE 2.10.4: Illustration of why a positive value of Δk is desirable in harmonic generation with focused laser beams. (a) Wavevector diagram for third-harmonic generation with Δk positive. Even though the process is phase mismatched, the fundamental beam contains an angular spread of wavevectors and the phase-matched process illustrated in (b) can occur with high efficiency. (c) Conversely, for Δk negative, efficient harmonic generation cannot occur.

in passing through its focus. This effect is known as the phase anomaly and was first studied systematically by Gouy (1890). For the case of nonlinear optics, this effect has important consequences over and above the phase shift imparted to the transmitted light beam, because in general the nonlinear polarization $p = \epsilon_0 \chi^{(q)} A_1^q$ will experience a phase shift that is q times larger than that experienced by the incident wave of amplitude A_1. Consequently, the nonlinear polarization will be unable to couple efficiently to the generated wave of amplitude A_q unless a wavevector mismatch Δk is introduced to compensate for the phase shift due to the passage of the incident wave through its focus. The reason why Δk should be positive in order for this compensation to occur can be understood intuitively in terms of the argument presented in Fig. 2.10.4.

Boyd and Kleinman (1968) have considered how to adjust the focus of the incident laser beam to optimize the efficiency of second-harmonic generation. They find that the highest efficiency is obtained when beam walkoff effects (mentioned in Section 2.3) are rendered negligible, when the incident laser beam is focused so that the beam waist is located longitudinally at the center of the crystal and the ratio L/b is equal to 2.84, and when the wavevector mismatch is set equal to $\Delta k = 3.2/L$. In this case, the power generated at the second-harmonic frequency is equal to

$$\mathcal{P}_{2\omega} = K\left[\frac{128\pi^2\omega_1^3 d_{\text{eff}}^2 L}{c^4 n_1 n_2}\right]\mathcal{P}_\omega^2. \tag{2.10.14}$$

Here K is a numerical constant that depends on the system of units in which this equation is evaluated. For the Gaussian system, which was used in the original work, $K = 1.068$. In ad-

dition, Boyd and Kleinman show heuristically that other parametric processes, such as sum- and difference-frequency generation, are optimized by choosing the same confocal parameter for both input waves and applying the same criteria used to optimize second-harmonic generation. The effects of focusing on various third-order processes have been analyzed by Bjorklund (1975).

2.11 Nonlinear Optics at an Interface

There are certain nonlinear optical processes that can occur at the interface between two dissimilar optical materials. Two such examples are shown schematically in Fig. 2.11.1. Part (a) shows an optical wave falling onto a second-order nonlinear optical material. We saw earlier (in Section 2.7) how to predict the amplitude of the second-harmonic wave generated in the forward direction. But in fact, a much weaker second-harmonic wave is generated in reflection at the interface separating the two materials. We shall see in the present section how to predict the intensity of this reflected harmonic wave. Part (b) of the figure shows a wave falling onto a centrosymmetric nonlinear optical material. Such a material cannot possess a bulk second-order nonlinear optical susceptibility, but the presence of the interface breaks the inversion symmetry for a thin region (of the order of one molecular diameter in thickness) near the interface, and this thin layer can emit a second-harmonic wave. The intensity of the light emitted by this surface layer depends sensitively on the structural properties of the surface and especially upon

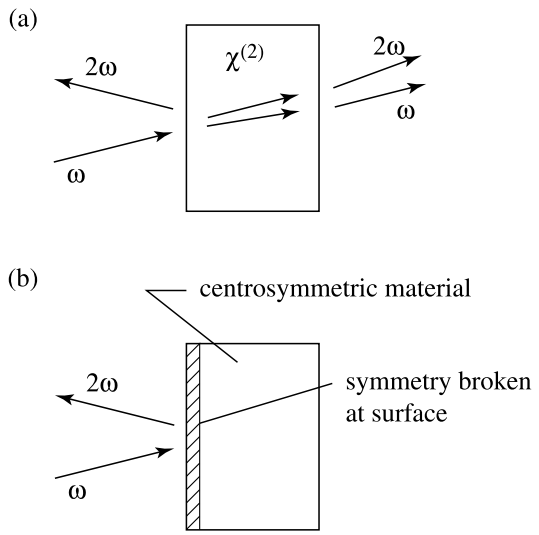

FIGURE 2.11.1: Illustration of second-harmonic generation in reflection at the surface of (a) a second-order nonlinear optical material and (b) a centrosymmetric nonlinear optical material.

the presence of molecules absorbed onto the surface. For this reason surface second-harmonic generation is an important diagnostic method for studies in surface science.

Let us consider in greater detail the situation illustrated in part (a) of Fig. 2.11.1. We assume that the wave at the fundamental frequency incident on the interface can be described by

$$\tilde{\mathbf{E}}_{\mathrm{i}}(\mathbf{r},t)=\mathbf{E}_{\mathrm{i}}(\omega_{\mathrm{i}})e^{-i\omega_{\mathrm{i}}t}+\text{c.c.}\quad\text{where}\quad\mathbf{E}_{\mathrm{i}}(\omega_{\mathrm{i}})=\mathbf{A}_{\mathrm{i}}(\omega_{\mathrm{i}})e^{i\mathbf{k}_{\mathrm{i}}(\omega_{\mathrm{i}})\cdot\mathbf{r}}. \tag{2.11.1}$$

This wave will be partially reflected and partially transmitted into the nonlinear optical material. Let us represent the transmitted component as

$$\mathbf{E}_{\mathrm{T}}(\omega_{\mathrm{i}})=\mathbf{A}_{\mathrm{T}}(\omega_{\mathrm{i}})e^{i\mathbf{k}_{\mathrm{T}}(\omega_{\mathrm{i}})\cdot\mathbf{r}}, \tag{2.11.2}$$

where the amplitude $\mathbf{A}_{\mathrm{T}}(\omega_{\mathrm{i}})$ and propagation direction $\mathbf{k}_{\mathrm{T}}(\omega_{\mathrm{i}})$ can be determined from the standard Fresnel equations of linear optics. For simplicity, in the present discussion we ignore the effects of birefringence; we note that birefringence vanishes identically in crystals (such as GaAs) that are noncentrosymmetric yet possess a cubic lattice. The transmitted fundamental wave will create a nonlinear polarization at frequency $\omega_{\mathrm{s}}=2\omega_{\mathrm{i}}$ within the medium that we represent as

$$\tilde{\mathbf{P}}(\mathbf{r},t)=\mathbf{P}e^{-i\omega_{\mathrm{s}}t}+\text{c.c. where }\mathbf{P}=\mathbf{p}e^{i\mathbf{k}_{\mathrm{s}}(\omega_{\mathrm{s}})\cdot\mathbf{r}}\text{ and }\mathbf{p}=\hat{\mathbf{p}}\epsilon_0\chi_{\mathrm{eff}}^{(2)}A_{\mathrm{T}}^2(\omega_{\mathrm{i}}) \tag{2.11.3}$$

where $\mathbf{k}_{\mathrm{s}}(\omega_{\mathrm{s}})=2\mathbf{k}_{\mathrm{T}}(\omega_{\mathrm{i}})$ and where $\hat{\mathbf{p}}$ is the unit vector $\hat{\mathbf{p}}=\mathbf{p}/|\hat{\mathbf{p}}|$.

The details of the ensuing analysis differ depending upon whether $\mathbf{p}$ lies within or is perpendicular to the plane of incidence. Here we treat only the case of $\mathbf{p}$ perpendicular to the plane of incidence (also known as the TE geometry); a treatment of the other case can be found for instance in Bloembergen and Pershan (1962) or in Shen (1984b). As described by Eq. (2.1.23), this nonlinear polarization will give rise to radiation at the second-harmonic frequency ω_{s}. The generation of this radiation is governed by the wave equation in the form

$$\nabla^2\mathbf{E}(\omega_{\mathrm{s}})+\left[\epsilon(\omega_{\mathrm{s}})\omega_{\mathrm{s}}^2/c^2\right]\mathbf{E}(\omega_{\mathrm{s}})=-\left(\omega_{\mathrm{s}}^2/\epsilon_0c^2\right)\mathbf{p}_{\perp}e^{i\mathbf{k}_{\mathrm{s}}\cdot\mathbf{r}} \tag{2.11.4}$$

where $\mathbf{p}_{\perp}$ is the component of $\mathbf{p}$ perpendicular to the plane of incidence. Here $\epsilon(\omega)$ is taken to be $\epsilon_T(\omega)$ in the nonlinear medium and as $\epsilon_R(\omega)$ in the linear medium. The formal solution to this equation consists of a particular solution plus a general solution to the homogeneous version of this equation obtained by setting its right-hand side equal to zero. It turns out that we can meet all of the appropriate boundary conditions by assuming that the homogeneous solution is an infinite plane wave of as yet unspecified amplitude $\mathbf{A}_{\mathrm{T}}(\omega_{\mathrm{s}})$ and wavevector $\mathbf{k}_{\mathrm{T}}(\omega_{\mathrm{s}})$. We thus represent the solution to Eq. (2.11.4) as

$$\mathbf{E}_{\mathrm{T}}(\omega_{\mathrm{s}})=\mathbf{A}_{\mathrm{T}}(\omega_{\mathrm{s}})e^{i\mathbf{k}_{\mathrm{T}}(\omega_{\mathrm{s}})\cdot\mathbf{r}}+\frac{(\omega_{\mathrm{s}}^2/\epsilon_0c^2)}{|k_{\mathrm{s}}|^2-|k_{\mathrm{T}}(\omega_{\mathrm{s}})|^2}\,\mathbf{p}_{\perp}e^{i\mathbf{k}_{\mathrm{s}}\cdot\mathbf{r}}, \tag{2.11.5}$$

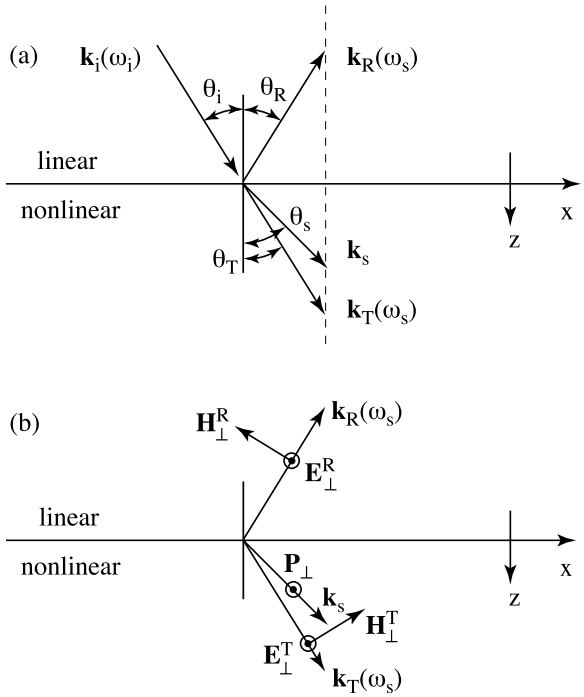

FIGURE 2.11.2: (a) Geometry showing the creation of a transmitted and reflected second-harmonic wave at the surface of a second-order nonlinear optical material. (b) Definition of the electric and magnetic field vectors for the case in which **P** is perpendicular to the plane of incidence.

where the second term on the right-hand side represents the particular solution, with $k_s = \sqrt{\epsilon(\omega_s)}\omega_s/c$, and with $|k_T(\omega_s)|^2 = \epsilon_T(\omega_s)\,\omega_s^2/c^2$. The electromagnetic boundary conditions at the interface require that the components of **E** and of **H** tangential to the plane of the interface be continuous. These boundary conditions can be satisfied only if we postulate the existence of a reflected, second-harmonic wave that we represent as

$$\mathbf{E}_R(\omega_s) = \mathbf{A}_R(\omega_s)e^{i\mathbf{k}_R(\omega_s)\cdot\mathbf{r}}. \tag{2.11.6}$$

In order that the boundary conditions be met at each point along the interface, it is necessary that the nonlinear polarization of wavevector $\mathbf{k}_s = 2\mathbf{k}_T(\omega_i)$, the transmitted second-harmonic wave of wavevector $\mathbf{k}_T(\omega_s)$, and the reflected second-harmonic wave of wavevector $\mathbf{k}_R(\omega_s)$ have identical wavevector components along the plane of the interface. This situation is illustrated in Fig. 2.11.2, where we let x be a coordinate measured along the interface in the plane of incidence and let z denote a coordinate measured perpendicular to the plane of incidence. We thus require that

$$k_x^s = k_{R,x}(\omega_s) = k_{T,x}(\omega_s) \tag{2.11.7}$$

(note that $k_x^{\mathrm{s}} \equiv 2k_{\mathrm{T},x}(\omega_{\mathrm{i}})$). Furthermore, we can express the magnitude of each of the propagation vectors in terms of the dielectric constant of each medium as

$$k_{\mathrm{T}}(\omega_{\mathrm{s}}) = \epsilon_{\mathrm{T}}^{1/2}(\omega_{\mathrm{s}})\ \omega_{\mathrm{s}}/c, \tag{2.11.8a}$$

$$k_{\mathrm{R}}(\omega_{\mathrm{s}}) = \epsilon_{\mathrm{R}}^{1/2}(\omega_{\mathrm{s}})\ \omega_{\mathrm{s}}/c, \tag{2.11.8b}$$

$$k_{\mathrm{i}}(\omega_{\mathrm{i}}) = \epsilon_{\mathrm{R}}^{1/2}(\omega_{\mathrm{i}})\ \omega_{\mathrm{i}}/c, \tag{2.11.8c}$$

where, as before, ϵ_{R} denotes the dielectric constant of the linear, incident medium and ϵ_{T} denotes the linear dielectric constant of the nonlinear medium. For mathematical convenience, we also introduce a fictitious dielectric constant ϵ_s associated with the nonlinear polarization defined such that

$$k_{\mathrm{s}} = \epsilon_{\mathrm{s}}^{1/2}\omega_{\mathrm{s}}/c. \tag{2.11.9}$$

From Eqs. (2.11.7) through (2.11.9) we can readily determine expressions relating the angles θ_{i}, θ_{R}, θ_{s}, and θ_{T} (see Fig. 2.11.2), which are given by

$$\epsilon_{\mathrm{R}}^{1/2}(\omega_{\mathrm{i}})\sin\theta_{\mathrm{i}} = \epsilon_{\mathrm{R}}^{1/2}(\omega_{\mathrm{s}})\sin\theta_{\mathrm{R}} = \epsilon_{\mathrm{T}}^{1/2}(\omega_{\mathrm{s}})\sin\theta_{\mathrm{T}} = \epsilon_s^{1/2}\sin\theta_{\mathrm{s}}. \tag{2.11.10}$$

This equation can be considered to be the nonlinear optical generalization of Snell's law.

We next apply explicitly the boundary conditions at the interface between the linear and nonlinear medium. According to Eq. (2.11.5), $\mathbf{p}_\perp$ will lead to the generation of an electric field in the $E_\perp = E_y$ direction, and in accordance with Maxwell's equations the associated magnetic field will lie in the xz plane (see part (b) of Fig. 2.11.2). The continuity of the tangential components of $\mathbf{E}$ and $\mathbf{H}$ then leads to the equations

$$\begin{aligned} E_y: \quad & A_\perp^{\mathrm{R}}(\omega_{\mathrm{s}}) = A_\perp^{\mathrm{T}}(\omega_{\mathrm{s}}) + p_\perp/\big[\epsilon_0(\epsilon_s - \epsilon_{\mathrm{T}}(\omega_{\mathrm{s}}))\big], \\ H_x: \quad & -\epsilon_{\mathrm{R}}^{1/2}(\omega_{\mathrm{s}})A_\perp^{\mathrm{R}}(\omega_{\mathrm{s}})\cos\theta_{\mathrm{R}} = \epsilon_{\mathrm{T}}^{1/2}(\omega_{\mathrm{s}})A_\perp^{\mathrm{T}}(\omega_{\mathrm{s}})\cos\theta_{\mathrm{T}} \\ & \quad + p_\perp\cos\theta_s\epsilon_s^{1/2}\big/\big[\epsilon_0(\epsilon_s - \epsilon_{\mathrm{T}}(\omega_{\mathrm{s}}))\big]. \end{aligned} \tag{2.11.11}$$

Here the perpendicular symbol $\perp$ is introduced as a reminder that we are treating the case in which the incident light is polarized perpendicular to the plane of incidence. These equations are readily solved simultaneously to obtain expressions for $A_\perp^{\mathrm{R}}$ and $A_\perp^{\mathrm{T}}$. These expressions are then introduced into Eqs. (2.11.5) and (2.11.6) to find that the transmitted and reflected fields are given by

$$\begin{aligned} E_\perp^{\mathrm{R}}(\omega_{\mathrm{s}}) &= \frac{-p_\perp e^{i\mathbf{k}_{\mathrm{R}}(\omega_{\mathrm{s}})\cdot\mathbf{r}}}{\epsilon_0[\epsilon_{\mathrm{T}}^{1/2}(\omega_{\mathrm{s}})\cos\theta_{\mathrm{T}} + \epsilon_{\mathrm{R}}^{1/2}(\omega_{\mathrm{s}})\cos\theta_{\mathrm{R}}]\big[\epsilon_{\mathrm{T}}^{1/2}(\omega_{\mathrm{s}})\cos\theta_{\mathrm{T}} + \epsilon_s^{1/2}\cos\theta_s\big]} \\ &\equiv A_\perp^{\mathrm{R}}(\omega_{\mathrm{s}})e^{i\mathbf{k}_{\mathrm{R}}(\omega_{\mathrm{s}})\cdot\mathbf{r}}, \end{aligned} \tag{2.11.12a}$$

$$E_{\perp}^{\mathrm{T}}(\omega_{\mathrm{s}}) = \frac{-p_{\perp}}{\epsilon_0[\epsilon_{\mathrm{T}}(\omega_{\mathrm{s}}) - \epsilon_s]}\left[e^{i\mathbf{k}_s\cdot\mathbf{r}} - \frac{\epsilon_s^{1/2}\cos\theta_s + \epsilon_{\mathrm{R}}^{1/2}(\omega_{\mathrm{s}})\cos\theta_{\mathrm{R}}}{\epsilon_{\mathrm{T}}^{1/2}(\omega_{\mathrm{s}})\cos\theta_{\mathrm{T}} + \epsilon_{\mathrm{R}}^{1/2}(\omega_{\mathrm{s}})\cos\theta_{\mathrm{R}}}\, e^{i\mathbf{k}_{\mathrm{T}}(\omega_{\mathrm{s}})\cdot\mathbf{r}}\right]. \tag{2.11.12b}$$

The transmitted second-harmonic wave is thus composed of a homogeneous contribution with propagation vector $\mathbf{k}_{\mathrm{T}}$ and an inhomogeneous wave with propagation vector $\mathbf{k}_s$. We see from Fig. 2.11.2 that $\mathbf{k}_s - \mathbf{k}_{\mathrm{T}}$ must lie in the z direction and is given by

$$\mathbf{k}_s - \mathbf{k}_{\mathrm{T}} = \Delta k\hat{z} = (\omega_{\mathrm{s}}/c)\left[\epsilon_{\mathrm{s}}^{1/2}\cos\theta_{\mathrm{s}} - \epsilon_{\mathrm{T}}^{1/2}(\omega_{\mathrm{s}})\cos\theta_{\mathrm{T}}\right]\hat{z}. \tag{2.11.13}$$

If this result is introduced into Eq. (2.11.12b), we can express the transmitted field in the form

$$\begin{aligned} E_{\perp}^{\mathrm{T}}(\omega_{\mathrm{s}}) &= \left[A_{\perp}^{\mathrm{R}}(\omega_{\mathrm{s}}) + \frac{(\omega_{\mathrm{s}}^2/\epsilon_0 c^2)p_{\perp}}{2k_{\mathrm{T}}(\omega_{\mathrm{s}})}\left(\frac{e^{i\,\Delta k z} - 1}{\Delta k}\right)\right]e^{i\mathbf{k}_{\mathrm{T}}(\omega_{\mathrm{s}})\cdot\mathbf{r}} \\ &\equiv A_{\perp}^{\mathrm{T}}(\omega_{\mathrm{s}})\, e^{i\mathbf{k}_{\mathrm{T}}(\omega_{\mathrm{s}})\cdot\mathbf{r}}. \end{aligned} \tag{2.11.14}$$

This equation has the form of a plane wave with a spatially varying amplitude; the spatial variation is a manifestation of imperfect phase matching of the nonlinear optical interaction. The present formalism demonstrates that the origin of the spatial variation associated with wavevector mismatch is the interference of the homogeneous and inhomogeneous solutions of the driven wave equation.

Let us interpret further the result given by Eq. (2.11.14). We assume that $\Delta k z$ is much smaller than unity for propagation distances z of interest. We then find that, correct to first order in Δk, the amplitude of the transmitted wave is given by

$$A_{\perp}^{\mathrm{T}}(\omega_{\mathrm{s}}) = A_{\perp}^{\mathrm{R}}(\omega_{\mathrm{s}}) + \frac{(\omega/c)^2 p_{\perp}(iz)}{2\epsilon_0 k_{\mathrm{T}}(\omega_{\mathrm{s}})} = A_{\perp}^{\mathrm{R}}(\omega_{\mathrm{s}}) + \frac{i(\omega/c)p_{\perp}z}{2\epsilon_0\epsilon^{1/2}(\omega_{\mathrm{s}})}. \tag{2.11.15}$$

We see that the amplitude of the generated wave grows linearly from its boundary value $A_{\perp}^{\mathrm{R}}(\omega_{\mathrm{s}})$. We also see from Eq. (2.11.12a) that $A_{\perp}^{\mathrm{R}}(\omega_{\mathrm{s}})$ will be given to order of magnitude by

$$A_{\perp}^{\mathrm{R}}(\omega_{\mathrm{s}}) \simeq -\frac{p_{\perp}}{4\epsilon_0\epsilon}, \tag{2.11.16}$$

where ϵ is some characteristic value of the dielectric constant of the region near the interface. On the basis of this result, Eq. (2.11.15) can be approximated as

$$A_{\perp}^{\mathrm{T}}(\omega_{\mathrm{s}}) \simeq -\frac{\pi p_{\perp}}{4\epsilon_0\epsilon}\left[1 - 2ik_{\mathrm{T}}(\omega_{\mathrm{s}})z\right]. \tag{2.11.17}$$

This result shows that the surface term makes a contribution comparable to that of the bulk term for a thickness t given by

$$t = \lambda/4\pi. \tag{2.11.18}$$

Let us next examine the situation of Fig. 2.11.1(b), which considers harmonic generation at the interface between two centrosymmetric media. An accurate treatment of such a situation would require that we know the nonlinear optical properties of the region near the interface at a molecular level, which is not possible at the present level of description (because we can rigorously deduce macroscopic properties from microscopic properties, but not vice versa). Nonetheless, we can make an order-of-magnitude estimate of the amplitude of the reflected wave for typical materials. Let us model the interface between two centrosymmetric materials as possessing a second-order susceptibility $\chi^{(2)}$ confined to a thickness of the order of a molecular dimension a_0. Here $\chi^{(2)}$ is a typical value of the second-order susceptibility of a noncentrosymmetric material. This assumption taken in conjunction with Eq. (2.11.18) leads to the prediction

$$\begin{aligned} A_{\perp}^{\mathrm{T}}(\text{centrosymmetric}) &= \frac{4\pi a_0}{\lambda} A_{\perp}^{\mathrm{T}}(\text{noncentrosymmetric}) \\ &\simeq 10^{-3} A_{\perp}^{\mathrm{T}}(\text{noncentrosymmetric}). \end{aligned} \tag{2.11.19}$$

This result is in agreement with the predictions of more detailed models (see, for instance, Mizrahi and Sipe, 1988b).

2.12 Advanced Phase Matching Methods

Types of Phase Matching

In the examples given thus far in the present chapter, we have been considering collinear phase matching, which is illustrated for sum-frequency generation in Fig. 2.12.1(a). More generally, one can consider noncollinear phase matching, also known as vector phase matching, which is illustrated in Fig. 2.12.1(b). A subtlety occurs when we allow the possibility of a wavevector mismatch, as shown in Figs. 2.12.1(c) and (d). For the case of a vector interaction (Fig. 2.12.1(d)), we see that the wavevector mismatch

$$\Delta\mathbf{k} = \mathbf{k}_1 + \mathbf{k}_2 - \mathbf{k}_3 \tag{2.12.1}$$

can have both longitudinal and transverse components. When working in the paraxial approximation, one often assumes that the transverse components of $\Delta\mathbf{k}$ must vanish so that $\Delta\mathbf{k}$ has a component only along the direction of propagation. We note that this assumption is rigorously true for plane waves of infinite transverse extent, as there cannot be any uncertainty in the transverse wavevector in this case.

We now turn to the case of angle phase matching in birefringent crystals and point out some additional behavior. In Fig. 2.12.2 we show plots of the refractive index as a function of the

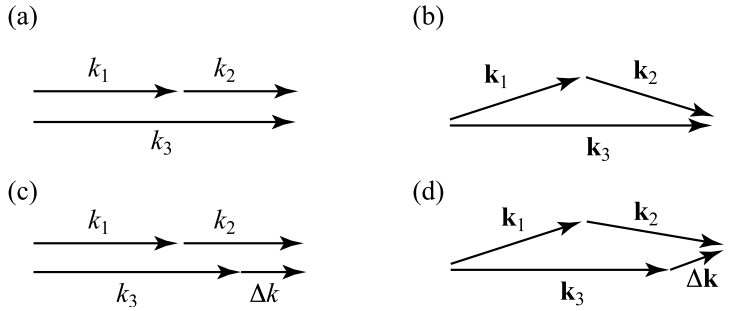

FIGURE 2.12.1: (a) Collinear phase matching; (b) noncollinear (vector) phase matching. (c) and (d) Three wave interactions with a wavevector mismatch.

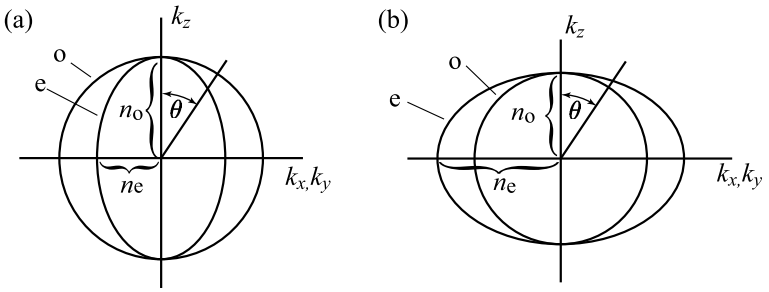

FIGURE 2.12.2: Refractive index surfaces for (a) negative and (b) positive uniaxial crystals. These curves show how the refractive index varies as a function of the propagation direction (**k**-vector direction) within the crystal.

propagation direction through the crystal.* We shall find that curves of the sort are extremely useful in understanding the nature of phase matching by means of angle tuning.

Beam Walk-Off Effects

We next describe a feature of birefringence phase matching that can under many circumstances limit the efficiency of the nonlinear process. In general, the wave vector **k** and the Poynting vector **S** are not parallel to one another in an anisotropic medium, as illustrated in Fig. 2.12.3. We reach this conclusion by first recalling the relation $\mathbf{S} = \mathbf{E} \times \mathbf{H}$, which shows that **S** must be perpendicular to the **E**. However, the Maxwell equation $\nabla \cdot \mathbf{D} = 0$ (written for a medium without free charges) leads to the transversality condition that **k** must be perpendicular

* These plots should not to be confused with the index ellipsoid, which plays an important role in the theory of crystal optics. Since $k = n\omega/c$, the plots of Fig. 2 have the same shape as a plot of **k** as a function of propagation direction for constant frequency ω. These plots are known as a plots of the normal surface or of the **k** surface. The relation between the **k** surface and the index ellipsoid are well explained in Saleh and Teich (2007) and in Zernike and Midwinter (1973b).

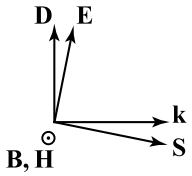

FIGURE 2.12.3: Orientation of the **E**, **D**, **B**, **H**, **k**, and **S** vectors in an anisotropic material.

to **D**. Because **D** and **E** are not in general parallel in a anisotropic medium, **k** and **S** are also generally not parallel. These vectors are parallel only for beams of ordinary polarization or, for extraordinary polarization, for propagation along the optic axis or for propagation perpendicular to it. Phase-matching conditions dictate the directions of the **k** vectors, but energy flow occurs in the direction of the Poynting vector **S**. Thus the interacting beams tend to walk away from each other as they propagate. The consequences of this beam walk-off are slightly different for type-I and type-II interactions. The consequences tend to be more severe for type-II interactions, because the two input beams can walk so far away from one another that they no longer overlap within the nonlinear material.

Critical and Non-Critical Phase Matching

An important distinction in nonlinear optics is that between critical and noncritical phase matching. We can understand this distinction by means of the example of infrared upconversion. Because infrared detectors tend to be much noisier than visible detectors, an infrared signal can sometimes be better detected by first converting it to a visible frequency by means of a nonlinear optical interaction (Boyd and Townes, 1977b; Vandevender and Kwiat, 2004). In the situation described in Fig. 2.12.4, a weak infrared signal beam of frequency ω_2 and wave vector $\mathbf{k}_2$ that one wants to detect is combined with a strong pump beam of frequency ω_1 and wave vector $\mathbf{k}_1$ in a second-order nonlinear optical crystal. The sum-frequency radiation at frequency $\omega_1 + \omega_2$ is then at an optical frequency. Oftentimes the signal to be detected has a broad angular extent. One wants to determine how large a divergence angle $\delta\theta$ can be used and still produce good conversion efficiency. Several possibilities exist. This interaction can be phase matched using standard angular phase matching, as shown in Fig. 2.12.4(b). The diagram is drawn for the case of type-I phase matching in a negative uniaxial crystal. In this situation, the wavevector mismatch increases approximately linearly as the direction of $\mathbf{k}_2$ is moved away from the phase-matching angle. This situation is known as that of critical phase matching, because the phase matching relation is satisfied only for one particular direction of the of $\mathbf{k}_2$ field. A more tolerant situation is that shown in part (c) of the figure. Through use of noncollinear phase matching, the curve for the directions of $\mathbf{k}_2$ can be made to be tangent to the curve for the sum frequency $\mathbf{k}_3$. In such a situation, the wavevector mismatch Δk increases only quadratically with the angular deviation of $\mathbf{k}_2$ from the phase-matching direction. This situation

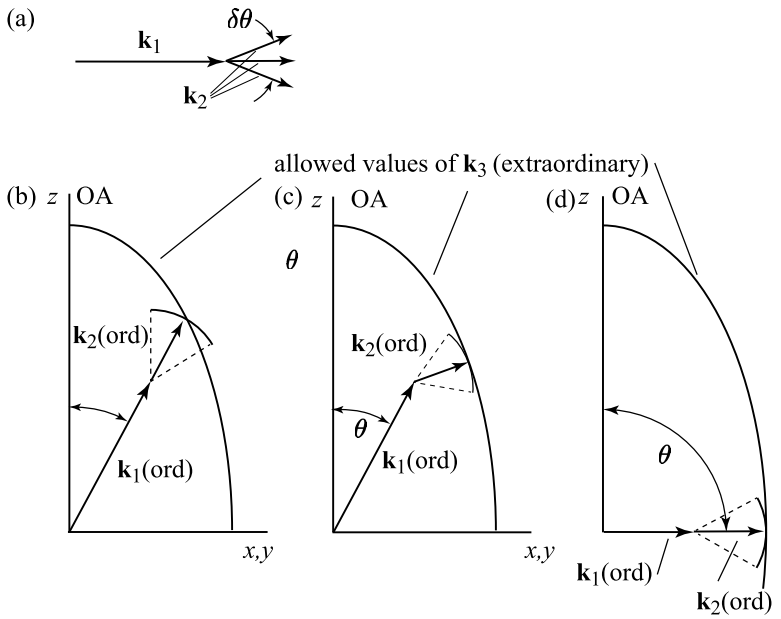

FIGURE 2.12.4: Distinction between critical and noncritical phase matching. (a) One wants to form the sum frequency of the pump wave $\mathbf{k}_1$ and a signal wave $\mathbf{k}_2$ of wide angular extend $\delta\theta$. (b) Critical phase matching; the phase mismatch scales approximately linearly with $\delta\theta$. (c) Noncritical phase matching; the phase mismatch scales only quadratically with $\delta\theta$. (d) Noncollinear phase matching at 90 degrees from the optical axis (OA). This situation is most desirable because walk-off is eliminated for $\theta = 90°$, and in addition the phase mismatch scales only quadratically with $\delta\theta$.

is known as noncritical phase matching. However, this situation still suffers from beam walk-off effects. The optimal strategy is to obtain phase matching at an angle of 90 degrees from the optic axis, as shown in part (d). This procedure leads to noncritical phase matching while avoiding beam walk-off effects.

Phase Matching of Spontaneous Parametric Down Conversion (SPDC)

We next consider the process of spontaneous parametric down conversion (SPDC). As illustrated in Fig. 2.12.5, SPDC is a process in which a single pump photon splits into two daughter photons conventionally known as the signal and idler photons. As this process is seeded only by the electromagnetic vacuum, it is a purely quantum process, and in fact the photons created by this process possess strong quantum properties. A complete treatment of the SPDC process would require us to develop a full quantum description of the electromagnetic field. While such a description is well understood, its treatment falls outside of the scope of the present book. We will instead rely on heuristic arguments to describe the correlations of the radiation cre-

ated by SPDC and refer the reader to several of the excellent text books that treat the quantum properties of nonlinear optical interactions. (Several suggestions are listed at the end of this chapter.)

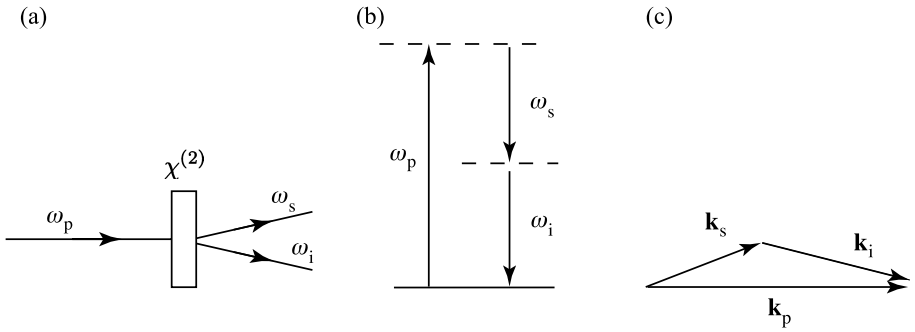

FIGURE 2.12.5: (a) Schematic illustration of the process of spontaneous parametric downconversion (SPDC). (b) Energy-level description and (c) wavevector description of the process.

The properties of SPDC are qualitatively very different for type-I and type-II phase matching. For definiteness, here we consider down-conversion in beta-barium borate (β-BBO), a negative uniaxial crystal.

We consider first the process of type-I SPDC in a negative uniaxial crystal. For simplicity, we here consider only the case of degenerate downconversion, that is, $\omega_i = \omega_s$. Fig. 2.12.6 shows schematically the observed behavior as one gradually rotates the crystal to vary the phase-matching condition. Part (a) shows the behavior when the pump angle θ in the notation of Fig. 2.12.5 is too small and the collinear wavevector mismatch $\Delta k = k_1 + k_2 - k_3 = n_1\omega_1 + n_2\omega_2 - n_3\omega_3$ is negative. No downconverted light is observed. Part (b) shows the behavior at the exact collinear phase matching angle. In this case, the downconverted light is observed only on the axis defined by the pump beam. Parts (c)–(e) show what happens when the pump angle is successively increased still further. In this case, phase matching is observed under noncollinear conditions. The generated light is now emitted in a cone surrounding the transmitted pump beam. The emitted light has strong quantum properties. Regions diametrically opposite on the emission cone are found to contain the same number of photons, to an accuracy much better than the inherent fluctuation in the number in either region. The sort of behavior has been observed experimentally in the high gain limit (Souto Ribeiro et al., 1997; Jedrkiewicz et al., 2006).

We next turn to the process of type-II SPDC, again for the case of a negative uniaxial crystal. Detailed analysis (Kwiat et al., 1995) shows that each of the signal and idler photons can again be emitted in the form of a ring pattern, but because they experience different refractive indices the two rings are centered on different propagation directions. The geometry of the SPDC process is illustrated in Fig. 2.12.7.

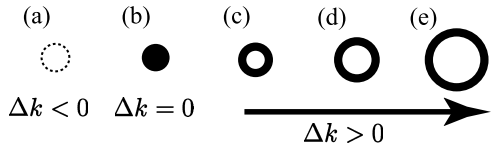

FIGURE 2.12.6: Behavior of spontaneous parametric downconversion in a type-I, negative uniaxial crystal as a function of the wave vector mismatch.

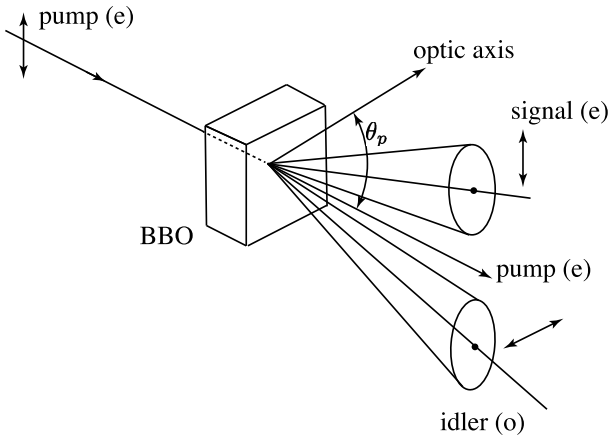

FIGURE 2.12.7: Geometry of spontaneous parametric downconversion in a negative uniaxial crystal for a type-II interaction.

Crucially, under certain phase matching conditions these two rings intersect at two locations. This sort of behavior is illustrated in Fig. 2.12.8. At these locations, the two photons are found to be entangled in their state of polarization. Entanglement in the present context has the following meaning. Although a photon detected in one of these regions has a 50/50 chance of having either the ordinary (o) of extraordinary (e) polarization, nonetheless, whenever the photon from one of the regions is found to be o polarized, the photon from the other region is found to be e polarized and vice versa.

Other geometries can also be used to produce polarization entanglement. One particularly useful procedure is the two-crystal procedure of Kwiat et al. (1999). This procedure uses two relatively thin crystals in close contact, each fabricated for type-I phase matching. The two crystals are rotated by 90 degrees with respect to one another, and the pump beam is polarized at 45 degrees to the principal axes of the two crystals. Each crystal produces light by SPDC, and the polarization of the light from each crystal is orthogonal to that of the other. Because the crystals are very thin, there is no way to know which crystal produced the light. The down-converted photons are thus entangled in their states of polarization. Specifically, if the light from one crystal has H (for horizontal) polarization and the light from the other has V (for vertical)

polarization, the quantum state of the polarization of the emitted light can be represented by

$$\Psi = \frac{HH + VV}{\sqrt{2}} \tag{2.12.2}$$

Polarization entanglement of this sort is found to have myriad applications in quantum information. Some examples are given in Giovannetti et al. (2004).

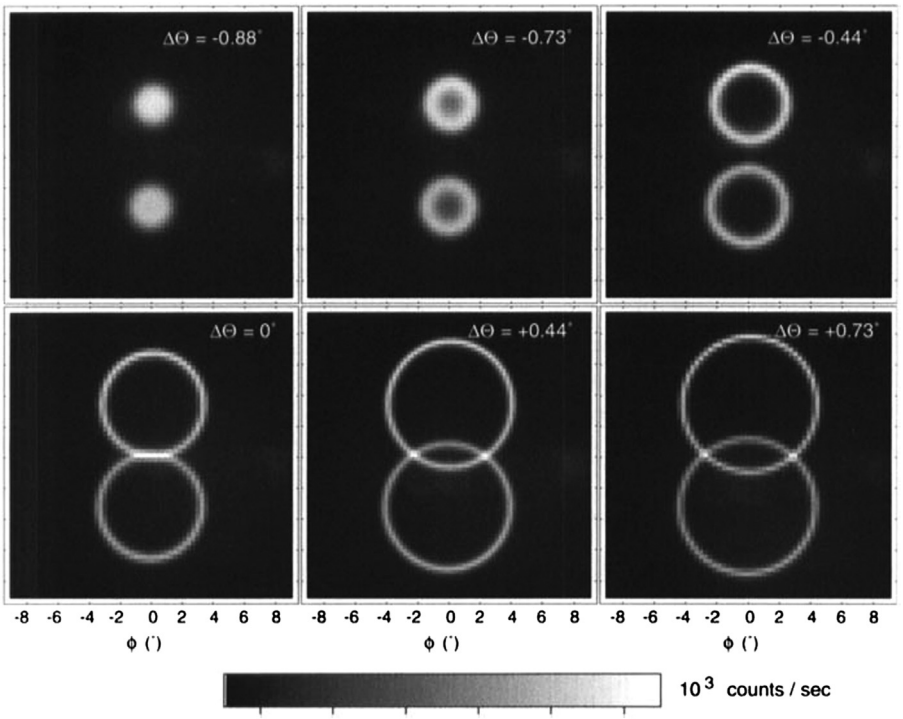

FIGURE 2.12.8: Behavior of spontaneous parametric downconversion in a type-I, negative uniaxial crystal as a function of the crystal rotation angle. For the two panels on the bottom right the two rings intersect at two locations. Polarization entanglement occurs under these circumstances. (Kurtsiefer et al., 2001).

Tilted-Pulse-Front Method for the Generation of THz Radiation

We next describe some of the special considerations that occur for the phase-matched generation of THz radiation. THz radiation is often generated by illuminating a second-order nonlinear optical material such as lithium niobate with a short, intense near-infrared (NIR) light pulse often generated by a Ti:sapph laser operating at 800 nm. The generation process is often referred to as optical rectification, although it is perhaps better described as a form of difference-frequency generation involving the process $\chi^{(2)}(\omega_{\mathrm{THz}}; \omega_{\mathrm{NIR}} + \omega_{\mathrm{THz}}, -\omega_{\mathrm{NIR}})$. Here

ω_{THz} is the THz frequency to be generated and ω_{NIR} is the nominal frequency of the near-infrared pump laser. We assume that both ω_{NIR} and $\omega_{\mathrm{NIR}} + \omega_{\mathrm{THz}}$ lie within the spectrum of the pump pulse.

A wavelength of 800 nm corresponds to a frequency of 375 THz, which is very much larger than that of the radiation to be generated at approximately 1 THz. It is because of this great frequency difference that phase matching can become qualitatively different from that of visible-frequency nonlinear optics.

The phase matching condition for such a process, assumed for the present to be collinear, is given by

$$\Delta k = k(\omega_{\mathrm{NIR}} + \omega_{\mathrm{THz}}) - k(\omega_{\mathrm{NIR}}) - k(\omega_{\mathrm{THz}}) = 0. \tag{2.12.3}$$

This equation can be written in terms of refractive indices as

$$\Delta k = \frac{1}{c}[n(\omega_{\mathrm{NIR}} + \omega_{\mathrm{THz}})(\omega_{\mathrm{NIR}} + \omega_{\mathrm{THz}}) - n(\omega_{\mathrm{NIR}})\omega_{\mathrm{NIR}} - n(\omega_{\mathrm{THz}})\omega_{\mathrm{THz}}] = 0 \tag{2.12.4}$$

We now simplify this equation by expressing $n(\omega_{\mathrm{NIR}} + \omega_{\mathrm{THz}})$ as a power series in ω_{THz} to obtain $n(\omega_{\mathrm{NIR}}) + (dn(\omega_{\mathrm{NIR}})/d\omega_{\mathrm{NIR}})\omega_{\mathrm{THz}} = n_g(\omega_{\mathrm{NIR}})\omega_{\mathrm{THz}}$ where in the last form we have introduced the standard expression for the group index n_g. In addition, we drop the resulting term $n_g(\omega_{\mathrm{NIR}})\,\omega_{\mathrm{THz}}\,\omega_{\mathrm{THz}}$ because it is much smaller than the term $n_g(\omega_{\mathrm{NIR}})\,\omega_{\mathrm{THz}}\,\omega_{\mathrm{NIR}}$. With these substitutions the phase-matching condition becomes simply

$$n_g(\omega_{\mathrm{NIR}}) = n(\omega_{\mathrm{THz}}) \tag{2.12.5}$$

This result was first obtained by Nahata et al. (1996) who also demonstrated phase matching by this method using ZnTe as their nonlinear material. This result seems at first sight surprising, because one might think that a phase matching condition should depend only on phase velocities and not on a group velocity. This result can be understood intuitively by noting that a nonlinear optical processes driven by an intense short pulse can be thought of as impulsive processes. The short pulse excites each molecule which then "rings" and emits its own radiation. The nature of constructive interference for the emitted radiation depends on its phase velocity. However, the moment of time at which the impulsive excitation occurs depends on the group velocity.

The phase matching condition of Eq. (2.12.5) was derive under the assumption of collinear propagation. If the waves are not collinear, it is to be replaced by

$$n_g(\omega_{\mathrm{NIR}})\cos\gamma = n(\omega_{\mathrm{THz}}), \tag{2.12.6}$$

where γ is the angle between the two beams. One obtains this result by taking the projection of the group velocity of the excitation beam onto the direction of the phase velocity of the generated beam.

THz generation under noncollinear conditions often takes the form of emission in a Cherenkov cone. The basic mechanism is illustrated in Fig. 2.12.9(a). A short intense pulse of near-infrared radiation propagates through a second-order nonlinear crystal with group velocity $v_g(\omega_{\text{NIR}})$. Secondary waves are generated at each point along its trajectory, which interfere to form the cone-shaped radiation pattern. The condition for the constructive interference of the individual wavelets is that

$$\cos\theta_{\text{C}} = \frac{v_p(\omega_{\text{THz}})}{v_g(\omega_{\text{NIR}})}, \tag{2.12.7}$$

where θ_{C} is defined in the figure and is known as the Cherenkov angle and $v_p(\omega_{\text{THz}})$ is the phase velocity at the THz frequency. Note by comparison of Eq. (2.12.6) and Eq. (2.12.7) that the THz emission process is automatically phase matched for $\gamma = \theta_{\text{C}}$.

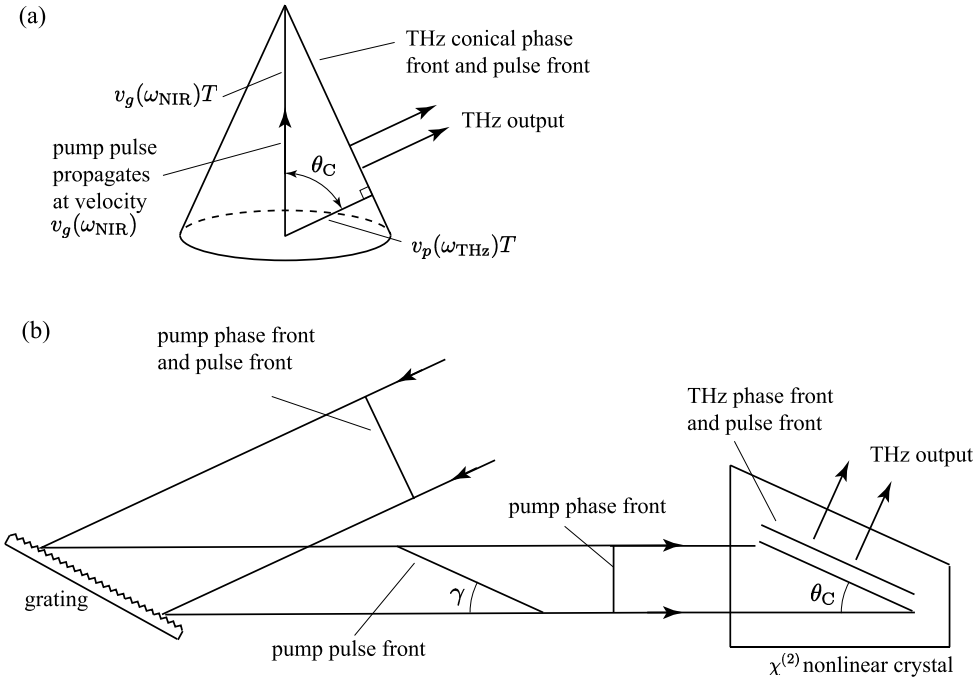

FIGURE 2.12.9: Methods for producing THz radiation through nonlinear optical interactions. (a) Cherenkov-cone generation. In time T, a short pulse of near-infrared radiation will travel a distance $v_g(\omega_{\text{NIR}})T$. In this time, the THz wavefront generated by the earliest-arriving part of the pulse will have traveled a distance $v_p(\omega_{\text{THz}})T$. The Cherenkov angle is thus given by $\theta_{\text{C}} = \cos^{-1}[v_p(\omega_{\text{THz}})/v_g(\omega_{\text{NIR}})]$. (b) Tilted-pulse-front method. When the incident plane-wave pump beam diffracts off a grating, the phase front and the pulse front are no longer parallel. By setting the pulse-front angle γ equal to the Cherenkov angle θ_{C}, one can ensure that there is no spatial walk-off between the pump pulse and the generated THz wave. For simplicity, the refraction of the pulse front at the entrance to the nonlinear crystal is ignored.

A limitation to the efficiency of THz generation based on the use of the interaction of Fig. 2.12.8(a) is the spatial walk-off of the two interacting beams. As illustrated in the figure, the THz radiation is emitted at nearly right angles to the propagation direction of the pump beam. As an example, for lithium niobate the NIR group index is given by $n_g(\omega_{\text{NIR}}) = 2.25$ and the THz phase index is given by $n(\omega_{\text{THz}}) = 4.96$ so that the Cherenkov angle is equal to 64 degrees (Hebling et al., 2008).

A solution to the problem of low conversion efficiency because of beam walk-off is the tilted pulse-front method, which has been described and implemented by Hebling et al. (2002, 2008). For a short optical pulse, the spatial extent of the pulse in the longitudinal direction is much smaller than that in the transverse directions. (One sometimes hears that ultrashort laser pulses are "flying pancakes.") The pulse front describes the instantaneous spatial distribution of pulse energy. The tilted pulse-front method is illustrated in Fig. 2.12.9(b). The near-infrared pump pulse is first diffracted from a grating, and as a result the wavefronts and pulse fronts are no longer parallel. The pump pulse then enters the nonlinear crystal, which is cut and oriented as shown in the figure. THz radiation is generated in the phase matched (Cherenkov) direction. The pulse fronts are oriented so that they coincide with the THz wave fronts, and as a result there is no spatial walk-off between the pump and generated THz radiation.

Problems

1. *Infrared upconversion.* One means of detecting infrared radiation is to first convert the infrared radiation to the visible by the process of sum-frequency generation. Assume that infrared radiation of frequency ω_1 is mixed with an intense laser beam of frequency ω_2 to form the upconverted signal at frequency $\omega_3 = \omega_1 + \omega_2$. Derive a formula that shows how the quantum efficiency for converting infrared photons to visible photons depends on the length L and nonlinear coefficient d_{eff} of the mixing crystal, and on the phase mismatch Δk. Estimate numerically the value of the quantum efficiency for upconversion of 10-μm infrared radiation using a 1-cm-long proustite crystal, 1 W of laser power at a wavelength of 0.65 μm, and the case of perfect phase matching and optimum focusing.
   [Ans.: $\eta_Q = 2\%$.]
2. *Sum-frequency generation.* Solve the coupled-wave equations describing sum-frequency generation (Eqs. (2.2.10) through (2.2.12b)) for the case of perfect phase matching ($\Delta k = 0$) but without making the approximation of Section 2.6 that the amplitude of the ω_2 wave can be taken to be constant.
   [Hint: This problem is very challenging. For help, see Armstrong et al. (1962).]
3. *Systems of units.* Rewrite each of the displayed equations in Sections 2.1 through 2.5 in the Gaussian system of units.

4. *Difference-frequency generation.* Solve the coupled-amplitude equations describing difference-frequency generation in the constant-pump limit, and thereby verify Eqs. (2.9.2) of the text. Assume that $\omega_1 + \omega_2 = \omega_3$, where the amplitude A_3 of the ω_3 pump wave is constant, that the medium is lossless at each of the optical frequencies, that the momentum mismatch Δk is arbitrary, and that in general there can be an input signal at each of the frequencies ω_1, ω_2, and ω_3. Interpret your results by sketching representative cases of the solution and by taking special limiting cases such as that of perfect phase matching and of only two input fields.
5. *Second-harmonic generation.* Verify that Eq. (2.7.29) possesses solutions of the sort shown in Fig. 2.7.2.
6. *Second-harmonic generation.* Solve the coupled-amplitude equations for the case of second-harmonic generation with the initial conditions $A_2 = 0$ but A_1 arbitrary at $z = 0$. Assume that Δk is arbitrary. Sketch how $|A(2\omega)|^2$ varies with z for several values of Δk, and thus verify the results shown in Fig. 2.7.2.
7. *Mode structure of an optical cavity.* Verify Eq. (2.9.11).
   [Ans.: Assume that the refractive index n is a function of ν and require that an integral number m of half wavelengths fit within the cavity of length L_c. Thus $m\lambda/2 = L_c$ or, since $\lambda = c/n\nu$, we obtain $n\nu = cm/2L_c$. We want to determine the frequency separation of adjacent modes. Thus, $\Delta(n\nu) = \Delta(cm/2L_c)$ where Δ refers to the change in the indicated quantity between adjacent modes. Note that $\Delta(n\nu) = n\Delta\nu + \nu\Delta n = n\Delta\nu + \nu(dn/d\nu)\Delta\nu = [n + \nu(dn/d\nu)]\Delta\nu$ and that $\Delta(cm/2L_c) = c/2L_c\Delta(m) = c/2L_c$. Thus,
   $$\Delta\nu = \frac{c}{2L_c(n + \nu\, dn/d\nu)} = \frac{v_g}{2L_c} = \frac{c}{2n_g L_c},$$
   where $v_g = c/[n + \nu(dn/d\nu)]$ is the usual expression for the group velocity and where $n_g = n + \nu(dn/d\nu)$ is the group index.]
8. *Mode structure of an optical cavity.* Generalize the result of the previous problem to the situation in which the cavity length is L but the material medium has length $L_c < L$.
9. *Quasi-phase-matching.* Generalize the discussion of the text leading from Eq. (2.4.1) to Eq. (2.4.6) by allowing the lengths of the inverted and noninverted sections of nonlinear optical material to be different. Let Λ be the period of the structure and l be the length of the inverted region. Show how each of the equations in this range is modified by this different assumption, and comment explicitly on the resulting modification to the value of d_Q and to the condition for the establishment of quasi-phase-matching.
10. *Gaussian laser beams.* Verify that Eqs. (2.10.4a) and (2.10.5a) are equivalent descriptions of a Gaussian laser beam, and verify that they satisfy the paraxial wave Eq. (2.10.3).
11. *Gaussian laser beams.* Verify the statement made in the text that the trial solution given by Eq. (2.10.9) satisfies the paraxial wave equation in the form of Eq. (2.10.7) if the amplitude $\mathcal{A}_q(z)$ satisfies the ordinary differential equation (2.10.10).

12. *Phase matching with focused beams.* Evaluate the integral appearing in Eq. (2.10.13a) and thereby verify Eq. (2.10.13b).
13. *Third-harmonic generation.* Assuming the condition of perfect phase matching, derive and solve exactly the coupled-amplitude equations describing third-harmonic generation. You may assume that the nonlinear optical material is lossless. Include in your analysis the processes described by the two susceptibility elements $\chi^{(3)}(3\omega;\omega,\omega,\omega)$ and $\chi^{(3)}(\omega;3\omega,-\omega,-\omega)$. Calculate the intensity of the third harmonic wave as a function of the length of the interaction region for the following two situations: (a) In the limit in which the undepleted pump approximation is valid. (b) For the general case in which the pump intensity cannot be assumed to remain constant.
14. *Poynting's theorem.* Derive the form of Poynting's theorem valid for a nonlinear optical material for which $\tilde{\mathbf{D}} = \epsilon_0\tilde{\mathbf{E}} + \tilde{\mathbf{P}}$ with $\tilde{\mathbf{P}} = \epsilon_0[\chi^{(1)}\tilde{\mathbf{E}} + \chi^{(2)}\tilde{\mathbf{E}}^2 + \chi^{(3)}\tilde{\mathbf{E}}^3]$. Assume that the material is nonmagnetic in the sense that $\tilde{\mathbf{B}} = \mu_0\tilde{\mathbf{H}}$.
15. *Backward second-harmonic generation.* Part (c) of Fig. 2.1.1 implies that second-harmonic generation is radiated in the forward but is not appreciably radiated in the backward direction. Verify that this conclusion is in fact correct by deriving the coupled-amplitude equation for a second-harmonic field propagating in the backward direction, and show that the amplitude of this wave can never become appreciable. (Note that a more rigorous calculation that reaches the same conclusion is presented in Section 2.11.)
16. *Second-harmonic generation.* Consider the process of second-harmonic generation both with $\Delta k = 0$ and $\Delta k \neq 0$ in a lossless material. State the conditions under which the following types of behavior occur: (i) The fundamental and second-harmonic fields periodically exchange energy. (ii) The second-harmonic field asymptotically acquires all of the energy. (iii) The fundamental field asymptotically acquires all of the energy. (iv) Part of the energy resides in each component, and this fraction does not vary with z.
17. *Manley–Rowe relations.* Derive the Manley–Rowe relations for the process of second-harmonic generation. The derivation is analogous to that presented in Section 2.5 for the process of sum-frequency generation.
18. *Phase-matching requirements.* Explain why processes such as second-harmonic generation can be efficient only if the phase-matching relation $\Delta k = 0$ is satisfied, whereas no such requirement occurs for the case of two-photon absorption.
19. *Elementary treatment of second-harmonic generation.* The treatment of second-harmonic generation presented in the text is in many ways too mathematically complicated to allow for a simple conceptual understanding of the process. As an alternative, simpler approach, carry through the suggestion presented the sentence that follows Eq. (2.7.12). In particular, solve Eq. (2.7.11) in the undepleted pump limit and then use this result to express the intensity of the generated field in terms of the intensity of the fundamental field, the length L of the interaction region, and the value Δk of the wavevector mismatch.

20. *Cascaded optical nonlinearities.* The intent of this problem is to develop an understanding of the phenomenon known as cascaded optical nonlinearities. By cascaded optical nonlinearities, one means that, through propagation, a second-order nonlinearity can mimic a third-order nonlinearity. In particular, in this problem you are to calculate the phase shift acquired by an optical wave in propagating through a second-order nonlinear optical material under conditions of nearly phase-matched second-harmonic generation, and to determine the conditions under which the phase shift acquired by the fundamental wave is approximately proportional to the product of the path length and the intensity.
To proceed, start for example with Eqs. (2.7.10) and (2.7.11), and show that one can eliminate A_2 to obtain the equation

$$\frac{d^2A_1}{dz^2} + i\Delta k\frac{dA_1}{dz} - \Gamma^2\left(1 - 2|A_1/A_0|^2\right)A_1 = 0,$$

where Γ is a constant (give an expression for it) and A_0 is the incident value of the fundamental field. Show that under proper conditions (give specifics) the solution to this equation corresponds to a wave whose phase increases linearly with the length L of the nonlinear material and with the intensity I of the incident wave.
21. *Optimum focusing and second-harmonic generation.* Explain why it is that under optimum focusing conditions the power generated at the second harmonic frequency scales linearly rather than quadratically with the length L of the nonlinear crystal. (See Eq. (2.10.14).)
22. *Harmonic generation with focused Gaussian beams.* Develop and elucidate a conceptual understanding of why the intensity of the generated harmonic signal vanishes whenever the phase mismatch factor ΔkL is negative or zero. (See Fig. 2.10.3.)
23. *Magnetic response.* Explain why it is that for most optical interactions, whether linear or nonlinear, the interaction results primarily from the electric field **E** and not the magnetic field **B** of the incident radiation.
24. *Efficiency of Second-Harmonic Generation.* Equation (2.10.14) gives the predicted efficiency for second-harmonic generation of Gaussian beams under conditions of optimum focusing. This equation was derived by Boyd and Kleinman (1968) in a calculation based on the Gaussian system of units. Repeat this calculation using the SI system of units. (Of course, the final result is necessarily the same, but the details of the calculation may seem to be quite different.)
25. *Size of a Gaussian laser beam.* Show that the fraction of the power of a Gaussian laser beam that is contained in an area of radius $w(z)$ centered on the beam axis is given by $1 - 1/e^2 = 0.865$.
26. *Coupled-amplitude equations for quasi phase matching.* Derive Eqs. (2.4.4). Note that the form of these equations at first sight may appear strange, but it is straightforward to show that they are correct.

References

General References

Armstrong, J.A., Bloembergen, N., Ducuing, J., Pershan, P.S., 1962. Phys. Rev. 127, 1918.
Born, M., Wolf, E., 1975. Principles of Optics. Pergamon Press, Oxford.
Boyd, R.W., Townes, C.H., 1977a. Appl. Phys. Lett. 31, 440.
Byer, R.L., Herbst, R.L., 1977. In: Shen, Y.R. (Ed.), Tunable Infrared Generation. Springer-Verlag, Berlin.
Giordmaine, J.A., Miller, R.C., 1965. Phys. Rev. Lett. 14, 973.
Giordmaine, J.A., Miller, R.C., 1966. Appl. Phys. Lett. 9, 298.
Hobden, M.V., Warner, J., 1966. Phys. Lett. 22, 243.
Klein, M.V., 1970. Optics. Wiley, New York.
Maker, P.D., Terhune, R.W., Nisenoff, M., Savage, C.M., 1962. Phys. Rev. Lett. 8, 21.
Manley, J.M., Rowe, H.E., 1959. Proc. IRE 47, 2115.
Midwinter, J.E., Warner, J., 1965. Br. J. Appl. Phys. 16, 1135.
Shen, Y.R., 1984a. The Principles of Nonlinear Optics. Wiley, New York.
Zernike, F., Midwinter, J.E., 1973a. Applied Nonlinear Optics. Wiley, New York.

Section 3: Phase-Matching

Jundt, D.H., 1997. Opt. Lett. 22, 1553.
Edwards, G.J., Lawrence, M., 1984. Opt. Quantum Electron. 16, 373.

Section 4: Quasi-Phase-Matching

Byer, R.L., 1997. J. Nonlinear Opt. Phys. Mater. 6, 549.
Fejer, M.M., Magel, G.A., Jundt, D.H., Byer, R.L., 1992. IEEE J. Quantum Electron. 28, 2631.
Feng, D., Ming, N.-B., Hong, J.-F., Yang, Y.-S., Zhu, J.-S., Yang, Z., Wang, Y.-N., 1980. Appl. Phys. Lett. 37, 607.
Grassani, D., Pfeiffer, M.H.P., Kippenberg, T.J., Brès, C.-S., 2019. Opt. Lett. 44, 106.
Khanarian, G., Norwood, R.A., Haas, D., Feuer, B., Karim, D., 1990. Appl. Phys. Lett. 57, 977.
Lim, E.J., Fejer, M.M., Byer, R.L., Kozlovsky, W.J., 1989. Electron. Lett. 25, 731.
Magel, G.A., Fejer, M.M., Byer, R.L., 1990. Appl. Phys. Lett. 56, 109.
Meyn, J.-P., Fejer, M.M., 1997. Opt. Lett. 22, 1214.
Myers, R.A., Mukherjee, N., Brueck, S.R.J., 1991. Opt. Lett. 16, 1732.
Szilagyi, A., Hordvik, A., Schlossberg, H., 1976. J. Appl. Phys. 47, 2025.
van der Poel, C.J., Bierlein, J.D., Brown, J.B., Colak, S., 1990. Appl. Phys. Lett. 57, 2074.
Vodopyanov, K.L., Levi, O., Kuo, P.S., Pinguet, T.J., Harris, J.S., Fejer, M.M., 2004. Opt. Lett. 29, 1912.
Yamada, M., Nada, N., Saitoh, M., Watanabe, K., 1993. Appl. Phys. Lett. 62, 435.

Section 7: Applications of Second-Harmonic Generation

Campagnola, P.J., Wei, M., Lewis, A., Loew, L.M., 1999. Biophys. J. 77, 3341.
Chaitanya Kumar, S., Samanta, G.K., Devi, Kavita, Ebrahim-Zadeh, M., 2011. Opt. Express 19, 11152.
Curley, P.F., Ferguson, A.I., White, J.G., Amos, W.B., 1992. Opt. Quantum Electron. 24, 851.
Gauderon, R., Lukins, P.B., Sheppard, C.J.R., 1998. Opt. Lett. 23, 1209.
Guo, Y., Ho, P.P., Savage, H., Harris, D., Sacks, P., Schantz, S., Liu, F., Zhadin, N., Alfano, R.R., 1997. Opt. Lett. 22, 1323.
Gustafsson, M.G.L., 2005. Proc. Natl. Acad. Sci. 102, 13081.
Mizrahi, V., Sipe, J.E., 1988a. J. Opt. Soc. Am. C 5, 660–667.
Moreaux, L., Sandre, O., Mertz, J., 2000. J. Opt. Soc. Am. B 17, 1685.
Muller, M., Squier, J., Wilson, K.R., Brakenhoff, G.J., 1998. J. Microsc. 191, 266.
Shen, Y.R., 1985. J. Vac. Sci. Technol. B 3, 1464–1466.
Shen, Y.R., 1989. Nature 337, 519–525.
Westphal, V., Hell, S.W., 2005. Phys. Rev. Lett. 94, 143903.
Yelin, D., Silberberg, Y., 1999. Opt. Express 5, 169.

Section 9: Optical Parametric Oscillators

Bosenberg, W.R., Pelouch, W.S., Tang, C.L., 1989. Appl. Phys. Lett. 55, 1952.
Bosenberg, W.R., Tang, C.L., 1990. Appl. Phys. Lett. 56, 1819.
Byer, R.L., Rabin, H., Tang, C.L. (Eds.), 1973. Treatise in Quantum Electronics. Academic Press, New York.
Ebrahimzadeh, M., Dunn, M.H., 2001. In: Handbook of Optics IV, 2nd ed.. McGraw-Hill, New York.
Edelstein, D.C., Wachman, E.S., Tang, C.L., 1989. Appl. Phys. Lett. 54, 1728.
Myers, L.E., Eckardt, R.C., Fejer, M.M., Byer, R.L., Bosenberg, W.R., Pierce, J.W., 1995. J. Opt. Soc. Am. B 12, 2102.
Smith, R.G., Geusic, J.E., Levinstein, J.H., Rubin, J.J., Singh, S., van Uitent, L.G., 1968. Appl. Phys. Lett. 12, 308.
Simon, U., Tittel, F.K., 1994. In: Hulet, R.G., Dunning, F.B. (Eds.), Methods of Experimental Physics, Vol. III. Academic Press, San Diego.

Section 10: Nonlinear Optical Interactions with Focused Gaussian Beams

Bjorklund, G.C., 1975. IEEE J. Quantum Electron. QE-11, 287.
Boyd, G.D., Kleinman, D.A., 1968. J. Appl. Phys. 39, 3597.
Gouy, C.R., 1890. Acad. Sci. Paris 110, 1251.
Kleinman, D.A., Ashkin, A., Boyd, G.D., 1966. Phys. Rev. 145, 338.
Kogelnik, H., Li, T., 1966. Appl. Opt. 5, 1550.
Ward, J.F., New, G.H.C., 1969. Phys. Rev. 185, 57.

Section 11: Nonlinear Optics at an Interface

Bloembergen, N., Pershan, P.S., 1962. Phys. Rev. 128, 602.
Shen, Y.R., 1984b. The Principles of Nonlinear Optics. Wiley-Interscience, New York. See especially Section 6.4.
Mizrahi, V., Sipe, J.E., 1988b. J. Opt. Soc. Am. B 5, 660.

Recommended Textbooks on Quantum Nonlinear Optics

Drummond, P.D., Hillary, M., 2014. The Quantum Theory of Nonlinear Optics. Cambridge University Press.
Gerry, C.C., Knight, P.L., 2005. Introductory Quantum Optics. Cambridge University Press.
Klyshko, D.N., 1988. Photons and Nonlinear Optics. Gordon and Breach, New York.
Scully, M.O., Zubairy, M.S., 1997. Quantum Optics. Cambridge University Press.

Books that Treat Crystal Optics

Saleh, B.E.A., Teich, M.C., 2007. Fundamentals of Photonics, second edition. John Wiley and Sons, Hoboken.
Zernike, F., Midwinter, J.E., 1973b. Applied Nonlinear Optics. John Wiley and Sons, New York.

Recommended Further Reading on Quantum Nonlinear Optics

Boyd, R.W., Townes, C.H., 1977b. Appl. Phys. Lett. 31, 440.
Giovannetti, V., Lloyd, S., Maccone, L., 2004. Science 306, 1330.
Jedrkiewicz, O., Brambilla, E., Bache, M., Gatti, A., Lugiato, L.A., Di Trapani, P., 2006. J. Mod. Opt. 53, 575.
Kurtsiefer, C., Oberparleiter, M., Weinfurter, H., 2001. J. Mod. Opt. 48, 199.
Kwiat, P.G., Mattle, K., Weinfurter, H., Zeilinger, A., Sergienko, A.V., Shih, Y., 1995. Phys. Rev. Lett. 75, 4337.
Kwiat, P.G., Waks, E., White, A.G., Appelbaum, I., Eberhard, P.H., 1999. Phys. Rev. A 60, R773(R).
Souto Ribeiro, P.H., Schwob, C., Maître, A., Fabre, C., 1997. Opt. Lett. 24, 1893.
Vandevender, A.P., Kwiat, P.G., 2004. J. Mod. Opt. 51, 1433.

Suggested Further Readings on THz Pulse Generation

Hebling, J., Almási, G., Kozma, I.Z., Kuhl, J., 2002. Opt. Express 10, 1161–1166.
Hebling, J., Yeh, K.-L., Hoffmann, Matthias C., Bartal, B., Nelson, K.A., 2008. J. Opt. Soc. Am. B 25, B6–B19.
Nahata, A., Weling, A.S., Heinz, T.F., 1996. Appl. Phys. Lett. 69.